GLIA

WILEY

Functional adaptation of glial cells at neuromuscular junctions in response to injury

Anna P. Perez-Gonzalez[1,2] | Frédéric Provost[1,2] | Isabelle Rousse[1,2] |
Roberta Piovesana[1,2] | Ouafa Benzina[1,2] | Houssam Darabid[1,2] |
Benoit Lamoureux[1,2] | Yu Shi Wang[1,2] | Danielle Arbour[1,2] | Richard Robitaille[1,2,3]

[1]Département de Neurosciences, Université de Montréal, Montréal, Québec, Canada

[2]Groupe de Recherche sur le Système Nerveux Central, Université de Montréal, Montréal, Québec, Canada

[3]Centre Interdisciplinaire de Recherche sur le Cerveau et l'apprentissage, Montréal, Québec, Canada

Correspondence
Danielle Arbour, Département de neurosciences, Université de Montréal, Montréal, Québec, Canada H3C 3J7.
Email: danielle.arbour@umontreal.ca

Abstract

Synaptic elements from neuromuscular junctions (NMJs) undergo massive morphological and functional changes upon nerve injury. While morphological changes of NMJ-associated glia in response to injury has been investigated, their functional properties remain elusive. Perisynaptic Schwann cells (PSCs), glial cells at the NMJ, are essential for NMJ maintenance and repair, and are involved in synaptic efficacy and plasticity. Importantly, these functions are regulated by PSCs ability to detect synaptic transmission through, notably, muscarinic (mAChRs) and purinergic receptors' activation. Using Ca^{2+} imaging and electrophysiological recordings of synaptic transmission at the mouse NMJ, we investigated PSC receptors activation following denervation and during reinnervation in adults and at denervated NMJs in an ALS mouse model ($SOD1^{G37R}$). We observed reduced PSCs mAChR-mediated Ca^{2+} responses at denervated and reinnervating NMJs. Importantly, PSC phenotypes during denervation and reinnervation were distinct than the one observed during NMJ maturation. At denervated NMJs, exogenous activation of mAChRs greatly diminished galectin-3 expression, a glial marker of phagocytosis. PSCs Ca^{2+} responses at reinnervating NMJs did not correlate with the number of innervating axons or process extensions. Interestingly, we observed an extended period of reduced PSC mAChRs activation after the injury (up to 60 days), suggesting a glial memory of injury. PSCs associated with denervated NMJs in an ALS model ($SOD1^{G37R}$ mice) did not show any muscarinic adaptation, a phenotype incompatible with NMJ repair. Understanding functional mechanisms that underlie this glial response to injury may contribute to favor complete NMJ and motor recovery.

KEYWORDS
amyotrophic lateral sclerosis, denervation, muscarinic receptors, neuromuscular junction, perisynaptic Schwann cells, purinergic receptors, reinnervation

---

------

1 | INTRODUCTION

Neuromuscular junctions (NMJs) can undergo injury/repair cycles during their lifetime. These cycles could modify the state of innervation and impact muscle function, highlighting the importance of understanding the underlying synaptic events involved in the denervation/reinnervation processes. While changes in presynaptic and postsynaptic elements have been explored, little is known about the functional changes of perisynaptic Schwann cells (PSCs), glial cells at the NMJ.

PSCs are major determinants of NMJ repair. For instance, they extend processes (called glial bridges) from denervated endplates in the direction of innervated ones to induce sprouting and guidance of the presynaptic nerve terminal towards the denervated endplate (Magill et al., 2007; O'Malley et al., 1999; Reynolds & Woolf, 1992; Son & Thompson, 1995a, 1995b). Interestingly, the extent of NMJ repair (number of glial bridges or nerve sprouting) is regulated by synaptic activity (Love et al., 2003; Tam & Gordon, 2003), suggesting that there is a link between PSCs ability to repair the NMJ and their detection of synaptic activity (Ko & Robitaille, 2015).

PSCs regulation mainly relies on muscarinic (mAChRs) and purinergic receptors (Rochon et al., 2001). These allow them to detect and modulate synaptic activity and plasticity in Ca^{2+} dependent-manner (Castonguay & Robitaille, 2001; Robitaille, 1998; Todd et al., 2010) driven by synaptic activity itself and by their own intrinsic properties (Arbour et al., 2015; Belair et al., 2010; Darabid et al., 2013; Rousse et al., 2010). Importantly, in vivo blockade of mAChRs induces the same modifications in PSCs phenotype that take place during NMJ reinnervation (i.e bridges and sprouting) (Wright et al., 2009). In addition, PSCs upregulate glial fibrillary acidic protein (GFAP) following nerve injury or blockade of neuronal activity. This is driven by mAChRs, but not purinergic receptors (Georgiou et al., 1994; Georgiou et al., 1999). While Ca^{2+} elevations are reliable reporters of the receptors' activity, the regulation of GFAP gene expression occurs in a Ca^{2+}-independent manner (Georgiou et al., 1999). As a whole, these observations suggest that PSC mAChRs activation may be reduced in a context of injury.

We used mouse nerve-muscle preparations to evaluate functional changes that occur in PSCs during dynamic changes underlying NMJ denervation and reinnervation in different injury contexts. We show that PSCs displayed an overall reduced muscarinic activation at denervated adult NMJs. Maintaining PSCs mAChR activation of PSCs following denervation reduced the expression of galectin-3, a phagocytosis marker. Importantly, both muscarinic and purinergic functional adaptations were altered at denervated NMJs in the mouse model of ALS, SOD1^{G37R} mice. At reinnervating NMJs, both muscarinic and purinergic receptors activation were reduced, but neither PSCs Ca^{2+} responses evoked by muscarine nor ATP were correlated with the number of axon(s) or process(es) extension. Finally, the reduced PSC mAChR activation was observed for as long as 60 days after injury, suggesting a glial memory of injury. These results provide insights into PSC functional properties during denervation and reinnervation at the NMJ, revealing unique PSC phenotypes. Understanding mechanisms

implicated in such plasticity could be essential to notably optimize proper reinnervation process in adulthood.

2 | METHODS

2.1 | Animals and surgical procedures

2.1.1 | Animals

Certain experiments were performed on CD1 mice (Charles River, Canada), which were used at ages from postnatal day 3 to adulthood (P3, P7, P14, P21 and P60). For experiments to study reinnervation (characterization and local application of agonists), adult (P60-180) C57BL6 and the transgenic mice homozygote for the jellyfish yellow fluorescent protein (Thy1-YFP, [B6.Cg-Tg(Thy1-YFP)16Jrs/J], stock number 003709; The Jackson laboratories; Bar Harbor, ME, USA) were used (Feng et al., 2000).

An ALS mouse model was used to study NMJ denervation in a pathological condition. Transgenic mice heterozygote for the human *SOD1* gene carrying the mutation G37R were purchased and maintained in a C57BL/6 genetic background in our animal facilities (SOD1^{G37R}, line 29; [B6.Cg-Tg(SOD1*G37R)29Dpr/J]; stock number 008229; Wong et al., 1995). To visualize MN axons and nerve terminals in the SOD1^{G37R} mice, we crossed mice expressing Thy1-YFP with SOD1^{G37R} mice (YFP.SOD1^{G37R}). SOD1^{G37R}, YFP.SOD1^{G37R} and their wild type littermates (WT and YFP.WT) were genotyped by PCR amplification for the human *SOD1* gene performed on tail biopsy samples taken at the time of weaning (mice weight >10 g). Disease onset and progression were assessed weekly by monitoring animal weight (beginning at P300), the presence of tremors and the lack of hind limb extension reflex. We refer to the onset of the disease by the peak of the body weight curve and to the early disease as a 10% loss from the peak body weight. In our animal facilities, the median age of onset of the symptomatic YFP.SOD1^{G37R} used in this study was 499 days (N = 29), while the median age of early disease was 600 days (N = 29) and average duration of early disease progression 78.4 ± 8.5 days (N = 29). YFP.SOD1^{G37R} were used when they reached between 10 and 15% loss of their peak body weight (P445-479; hereafter referred as P460) to ensure the presence of NMJ denervation. An autopsy was performed on every animal. Animals with either cancerous tissue or any signs of infection were discarded.

Only males were used in the present study. Mice had ad libitum access to fresh water and food. All experiments were performed in accordance with the guidelines of the Canadian Council of Animal Care and the Comité de déontologie de l'expérimentation sur les animaux of Université de Montréal.

2.1.2 | Chronic denervation

CD1 mice (P21) were anesthetized using 2% isoflurane in 97%–98% O_2 delivered through a mask. The lateral surface of the hind limb was

shaved and the skin covering the gastrocnemius muscle washed with an antiseptic solution and cut open. The *gastrocnemius* muscle was then gently lifted and a short length of the tibial nerve was resected to prevent reinnervation of the *soleus* (SOL) muscle (Denervated). The skin incision was closed with sutures. The contralateral side was sham-operated and served as control (Innervated). Mice were injected subcutaneously with buprenorphine ($0.1 \ \mu g \ g^{-1}$) for analgesia. Animals were kept warm to prevent hypothermia after the surgery. Experiments were performed 1 week following surgery.

2.1.3 | Sciatic nerve crush surgery

C57BL6 adult mice (P55-85) were anesthetized using 2% isoflurane in 97%–98% O_2 delivered through a mask. The skin in the posterior lower back of the trunk was shaved and washed with an antiseptic solution, a mix of 70% alcohol and povidone iodine solution. Skin was cut and the *biceps femoris* and *gluteus maximus* were then gently separated from each other to expose the sciatic nerve. The sciatic nerve was then crushed either twice for 10 s or once for 15 s using a Moria microserrated curved forceps (MC31) to ensure a complete denervation followed by reinnervation of the SOL muscle (Reinnervating). Skin was then closed with sutures and animals were kept warm to prevent hypothermia. Other animals served as control as the same procedure was performed except for the nerve crush manoeuver (Sham). Buprenorphine, ($0.1 \ \mu g \ g^{-1}$), was applied before the surgery, 6–8 h after the surgery, and the following day. Of note, we observed spontaneous muscle twitching from 4 days post-injury until day 14, thus limiting our ability to perform electrophysiological or Ca^{2+} imaging recordings during that period.

2.1.4 | In vivo intermuscular injections

We adapted the technique from Wright et al. (2009) to perform intermuscular injections. Mice were anesthetized with isoflurane. Under aseptic conditions, saline (0.9%) or muscarine chloride (10 μM; Sigma) was administered in the left leg (side of the injury) between the *gastrocnemius* and the *peroneus* muscles to target the SOL. We used sterile injection devices containing a small volume (BD Safety Glide Insulin Syringe, 31G, 3/10 ml). Muscarine was dissolved in 50 μl of physiological saline (0.9%) to minimize injury from volume pressure. Saline and muscarine were administered over a period of 5 min (10 μl/min). Animals were randomly assigned to the Saline or Muscarine group in a blinded manner. Injections were performed immediately after the sciatic nerve crush injury and every 5 h afterwards until 48 h post-injury. Mice were weighed before every injection to ensure a good follow-up of their overall health.

2.2 | *Soleus* nerve-muscle preparations

Adult mice were deeply anesthetized using a mixture of midazolam and hypnorn ($0.1 \ \mathrm{ml \ g^{-1}}$ dissolved in distilled water) administered

intraperitoneally or euthanized with a lethal dose of isoflurane. For pups, euthanasia was induced by a lethal intraperitoneal injection of a mixture of ketamine (15 mg/ml) and xylazine (1 mg/ml). Dissection of the SOL muscle with its innervation was performed under oxygenated (5% CO_2, 95% O_2) Rees' physiological solution containing (in mM): 110 NaCl, 5 KCl, 1 MgCl2, 25 NaHCO3, 2 CaCl2, 11 glucose, 0.3 glutamate, 0.4 glutamine, 5 BES, 4.34×10^{-7} cocarboxylase and 0.036 choline chloride. The pH of the oxygenated solution was 7.3. The muscle and its innervation were then pinned in a Sylgard-coated recording chamber and the cut end of the tibial nerve inserted in a suction-stimulating electrode.

2.3 | Ventral root-muscle preparations

To monitor synaptic transmission at polyinnervated NMJs following reinnervation, dissection of the three ventral roots (L4, L5 and L6) from which axons originate to innervate the SOL was performed as described by Darabid et al. (2013) and Darabid et al. (2018). This allowed us to independently stimulate the different inputs innervating the same NMJ undergoing polyinnervation and synaptic competition during reinnervation.

2.4 | Calcium imaging

We used Ca^{2+} elevations as reliable reporters of PSCs activity. We performed dynamic Ca^{2+} imaging of PSCs using the membrane-permeant Ca^{2+} indicators Fluo-4 AM (Invitrogen) or Rhod-3 AM (ThermoFisher). SOL muscles and their innervation were dissected and placed in oxygenated Rees' physiological containing 10 μM Fluo-4 AM or 5 μM Rhod-3 AM, 0.02% pluronic acid (Molecular Probes) and 1% DMSO (Sigma), referred to as the loading medium. This method is known to preferentially load PSCs at the NMJ (Arbour et al., 2015; Martineau et al., 2020). Alexa594 or Alexa647 conjugated α-Bungarotoxin (α-BTX; Invitrogen) was added to the loading medium for the last 10–30 min. This facilitated the identification of the NMJs, especially in pups at P3 and P7 and in reinnervating muscles, without interfering with PSCs excitability (Jahromi et al., 1992).

Preparations were perfused (2 ml/min) for at least 20 min before the start of experiments. For most experiments, extracellular solution was the normal Normal Rees' physiological solution combined with D-tubocurarine chloride to block muscle postsynaptic nicotinic receptors (nAChRs) and prevent muscle contractions. To evaluate the cholinergic contribution, an antagonist of muscarinic receptors, atropine (20 μM, Sigma), was added and bath applied for at least 40 min prior to the experiments. To test the purinergic contribution, a selective $P2Y_1$ (MRS 2179; 20, 40, 50 μM; Abcam) and A1 (DPCPX; 100 nM; Tocris Bioscience) antagonists were also bath applied for at least 20 min prior to the experiments.

PSCs Ca^{2+} responses were evoked by endogenous release of neurotransmitters evoked by motor nerve situations (50 Hz, 30 s) or by local applications of agonists using a glass microelectrode (5 MΩ)

positioned close to the NMJ. Agonists were applied by brief pulses of positive pressure (10–20 PSI, 150–200 ms) using a Picospritzer II (General Valve Corporation). Agonists (muscarine chloride, 10–20 μM; ATP, 10–20 μM; acetylcholine, 20 μM; Sigma) were prepared in the same extracellular solution used for the experiment. PSCs not responding to ATP application were not considered further for analysis. Only PSCs of one NMJ per muscle were imaged when motor nerve stimulation was used, while PSCs at several NMJs were imaged with agonist applications. A recovery of 20 min was allowed between each application when several applications were performed on the same cells. Changes in fluorescence were measured over PSCs soma and expressed as $\%\Delta F = ([F\text{-}F_0]/F_0)^*100$. Basal fluorescence was recorded for 30 s before either nerve stimulation or local application was performed. Experiments were discarded when baseline fluorescence was not stable or focus drift occurred. Software and hardware settings were standardized to achieve a similar range of basal fluorescence within a range of arbitrary units for each set of experiments.

Ca^{2+} imaging of PSCs was performed using different microscopes. As previously reported in other studies (Belair et al., 2010), the same system was used throughout for a given condition and its related control. The use of different imaging systems explains the difference in the size of Ca^{2+} responses observed in different conditions reported in this study. More specifically, for agonists applications during development, changes in fluorescence were imaged with a ×60 water immersion objective (Nikon Fluor) mounted on an E600N Nikon epifluorescent microscope equipped with a CCD-1300 camera (Princeton Instruments). Images were acquired using the Metafluor software. Excitation was achieved through a 450–490 nm filter and emitted fluorescence was detected using a long-pass filter with a cut-off at 520 nm. For the denervation experiments (tibial nerve cut surgery), changes in fluorescence were monitored using the 488 nm line of the argon/krypton ion laser of a Bio-Rad MRC 600 laser-scanning confocal microscope (Hercules, CA, USA). The laser was attenuated to 1% of its maximal intensity and emitted fluorescence was detected using a long-pass filter with a cut-off at 515 nm. Localisation of NMJs was achieved via transmitted light microscopy, using a ×40 water immersion objective (0.75NA: Olympus). For agonists applications during reinnervation in adulthood, excitation of the Ca^{2+} indicator was achieved using the 559 nm line of the diode laser (Rhod-3AM) of a FV1000 Olympus confocal microscope. Emitted fluorescence was detected with a 60X water immersion objective (0.90 NA; Olympus, Tokyo, Japan) and fed into a spectral window detector (570 nm and above). For all other experiments, changes in intracellular Ca^{2+} were monitored with an LSM 510 confocal laser-scanning microscope (Carl Zeiss, Canada) using a 40X water immersion objective (0.80NA: Zeiss) and the 488 nm line of the Argon laser (power at 0.5%; Fluo-4AM).

2.5 | Immunohistochemical labeling of NMJs

Immunofluorescence was performed on whole mount preparations to visualize the three components of the NMJ (PSCs, presynaptic terminal and nAChRs) as previously described (Arbour et al., 2015; Darabid et al., 2013). Briefly, SOL muscles were pinned in Sylgard-coated dishes and fixed with 4% formaldehyde (Mecalab, Canada) at room temperature for 10 min, rinsed with PBS and then permeabilized with 100% cold methanol for 6 min at $-20°C$. Blockade of nonspecific labeling was achieved by incubating the muscles in a solution containing 10% normal donkey serum (NDS; Jackson ImmunoResearch Laboratories) and 0.01% Triton X-100 for 20 min. PSCs were then labeled with a S100 rabbit antibody (1:250, DAKO) for 2 h at room temperature. After rinsing with PBS containing 0.01% Triton X-100, presynaptic terminals were labeled using two primary antibodies, a chicken anti-neurofilament M (1:2000, 212-901-D84, Rockland) and a mouse IgG1 anti-synaptic vesicular 2 (1:2000, AB_2315408, DSHB) for 2 h at room temperature. For some experiments, muscles were also incubated overnight at 4°C with a rat IgG2a anti-MAC-2 (galectin-3) antibody (1:250, clone M3/38, Cedarlane). Secondary antibodies (Alexa488 α-goat/FITC α-chicken or Alexa488 α-chicken/Alexa 488 α-mouse IgG1, Alexa647α-rat IgG or α-rabbit, 1:500, Jackson ImmunoResearch) were incubated together for 60 min at room temperature. Muscles were then rinsed again and incubated with α-BTX (Alexa594 or CF405, 0.75 μg/ml, ThermoFisher or Biotium, respectively) for 45 min at room temperature. All antibodies were diluted in a PBS containing 0.01% Triton X-100 and 2% NDS. Muscles were mounted in a Prolong Gold antifade medium or Prolong Diamond medium to preserve endogenous fluorescence of the YFP protein (Molecular probes by Life technologies) and all labeled elements of the NMJs were simultaneously visualized using a LSM 510, LSM 880 or a FV1000 Olympus confocal laser-scanning microscope (Carl Zeiss, Canada).

2.6 | Morphological and galectin-3 analyses

A morphological analysis was performed to determine the innervation status of NMJs following nerve crush injury (8-, 10-, 12-, 14- and 18-days post injury—DPI). For each NMJ, the presence of presynaptic elements over the nAChRs α-BTX-labeled endplate was determined and classified in four categories: denervated (no axonal label), partially innervated (partial presynaptic coverage of the endplate), mono-innervated (a single axon) or polyinnervated (at least two independent axons). At least 20 surface NMJs were analyzed per muscle. Data from Sham muscles were grouped together and compared to the nerve-crushed ones at different DPI.

In a subset of experiments, morphological analysis was performed on previously recorded NMJs (Ca^{2+} imaging). The unique pattern of the nAChRs revealed by the α-BTX staining of a given NMJ and the surrounding ones allowed us to create a map during the Ca^{2+} imaging experiment to retrieve each NMJ in a subsequent immunofluorescence imaging session.

Galectin-3 quantification was performed at the level of a single plane. A region of interest (ROI) was drawn around each PSC soma and the mean intensity of fluorescence (arbitrary units; a.u.) was

measured within this ROI with Image J software. The single plane where the mean intensity was the highest was selected for the analysis. As a control, the ROI was also transposed to the S100 staining to ensure its localization in PSCs soma. All parameters of image acquisition were set according to the Saline group and remained the same all along the images acquisition and for the Muscarine group.

2.7 | Electrophysiological recordings

Intracellular recordings of endplate potentials (EPPs) were performed at 28–30°C using glass microelectrodes (1.0 mm OD; WPI) pulled to 40–70 MΩ (filled with 3M KCl) with a P95 Brown-Flaming micropipette puller (Sutter Instruments). Synaptic responses were recorded using an Axoclamp 2B amplifier (Axon Instruments) or a Multiclamp 700B amplifier (Molecular Devices) and further amplified ($\times$100) and filtered (2 kHz) by a Warner Instruments amplifier. EPPs were digitized at 10 kHz with DigiData 1322A (Axon Instruments) and analyzed off line with pClamp 8.0 software (Axon Instruments). Normal Rees' physiological solution was perfused and muscle contractions were prevented by blocking nAChRs with D-tubocurarine chloride (2.0–3.0 μM; Millipore Sigma) or of μ-conotoxin GIIIB (3–4 μM; Cerdalane). The tip of the microelectrode was inserted into a muscle fiber near (~30 μm) an NMJ visualized using either a $\times$40 or a $\times$60 water immersion objective (respectively 0.8 NA, Carl Zeiss, Germany and 0.90 NA; Olympus, Japan). The SOL nerve (tibial) or a single ventral root was stimulated with square pulses of 0.1 ms duration (Master-8 stimulator; AMPI) at twice the threshold required to elicit an EPP. EPPs were recorded for 10 min while stimulating the nerve/root at 0.2 Hz. Recordings with a membrane potential more depolarized than −60 mV were discarded.

2.7.1 | Synaptic strength and plasticity of polyinnervated NMJs

All recordings of synaptic strength were obtained by perfusing at least 20 min prior to the recordings a modified Rees' physiological solution with a low Ca^{2+} (1 mM)/ high Mg^{2+} (6–7 mM) concentrations. This greatly reduced the level of transmitter release necessary for the quantal analysis (Darabid et al., 2013). No muscle contractions were observed in these conditions. EPPs were recorded for 10 min while stimulating a ventral root at 0.2 Hz. The synaptic strength of each nerve terminal innervating the same endplate was determined by independently stimulating individual ventral root innervating the NMJ. Synaptic strength was evaluated based on the failure method described by (Del Castillo & Katz, 1954) and it is expressed as the quantal content: m = Log e (#nerve impulses/#failures). The calculation of m was performed after the completion of the experiments. Hence, the synaptic strength of each nerve terminal was unknown to the experimenter during the experiments.

For the subsequent recordings of the synaptic plasticity, extracellular solution was changed for the normal Normal Rees' physiological solution combined with D-tubocurarine and perfused at least 20 min. The baseline of synaptic activity was recorded for each NMJ by independent stimulation of their respective ventral root for 10 min at 0.2 Hz. Then, a first root was stimulated 50 Hz for 30 s (high frequency stimulation, HFS) and after a 20 min rest period, the second one was stimulated and changes in synaptic activity was monitored for at least 20 min after the HFS. EPP amplitude is expressed as % amplitude change compared to baseline: (EPP amplitude in mV/mean baseline EPP amplitude in mV) $\times$ 100. Each point represents the mean amplitude of 24 EPPs (2 min).

2.8 | Statistical analyses

Results are presented as mean ± SEM. *N* represents the number of muscles from different animals (biological replicate number) and n the number of NMJs (morphological analysis and electrophysiological experiments) or PSCs (Ca^{2+} imaging experiments). Unless stated otherwise, all data were confirmed to normality using a Kolmogorov–Smirnov normality test. Due to the use of different experimental set-ups, comparisons were only made in the same experimental conditions. *Paired t-test* was used to compare two different conditions in the same animal (Denervated and Innervated) and *Unpaired t-test* or *Mann–Whitney test* was used to compare two different conditions (Sham and Reinnervating, Saline and Muscarine or YFP.SOD1^{G37R} Innervated/Devervated). *One-way ANOVA test* with *Tukey's multiple comparison* post hoc *tests* (synaptic plasticity and ages) or *Kruskal-Wallis test* with *Dunn's multiple comparison* post hoc *tests* (60–90 DPI) were used to compare several groups in the same experimental condition (agonist or antagonist). The correlation between two or multiple sets of data were evaluated with the Pearson's or Spearman's coefficient respectively. For the morphological analysis, *N* represents the number of muscles from different animals (biological replicate number) and n are the number of observations. The morphological data do not follow a Gaussian Distribution or have equal variance and symmetric between groups. Hence, a *generalized linear model* (GLM) was created to evaluate the effect of the DPI on the measured morphological criteria (Martineau et al., 2020; Tremblay et al., 2017). *Sequential Sidak Sig test* method was used to correct for multiple comparisons (hereafter referenced by *Sidak post-test*). All statistical tests were performed in GraphPad Prism software (version 9.3.0) except for the GLM analysis (SPSS software; v.24.0.0.0; IBM). Analyses were deemed significant at $p < .05$.

3 | RESULTS

PSC receptor activation represents a central element for appropriate regulation of NMJ maintenance, function and repair (Ko & Robitaille, 2015). Thus, we hypothesized that PSC properties will be altered in response to NMJ injury. We investigated the adaptation of PSCs at denervated and reinnervating NMJs.
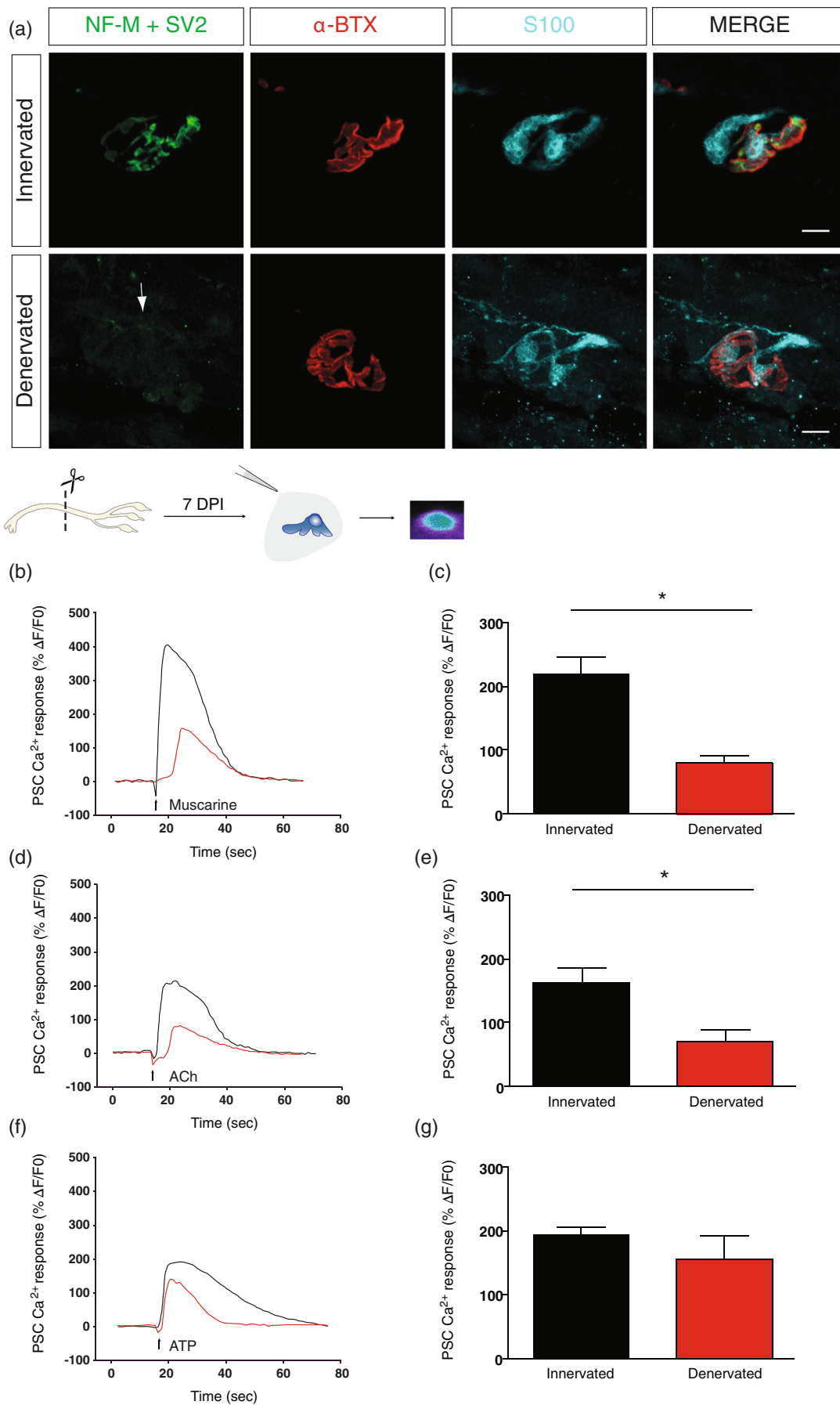
FIGURE 1 Legend on next page.

3.1 | Reduced PSCs muscarinic excitability, but not purinergic, at denervated NMJs

We first tested whether PSCs undergo functional changes following NMJ denervation. Since muscarinic antagonist induced an injury-like response of PSCs (Wright et al., 2009), we hypothesized that PSCs mAChR activation will be reduced at mature denervated NMJs.

The tibial nerve was resected to induce denervation at the SOL muscle and impide reinnervation. Complete denervation was confirmed 1 week later by the absence of muscle contractions upon the stimulation of the nerve stump confirmed under high magnification objective ($\times 40$ objective lens). Muscle contractions were never observed, not even in a restricted portion of the SOL muscle. We further confirmed NMJ denervation using immunohistochemical labeling of the three synaptic components of the NMJ. None of the endplates examined ($N = 7$, $n = 47$) showed any sign of innervation, as revealed by the absence of presynaptic labeling, 1 week after the surgery (Figure 1a). Hence, these preparations were considered denervated.

PSC receptor activation (mobilization of synaptic and extrasynaptic receptors by exogenous activation) at denervated NMJs was tested by local application of different agonists of muscarinic and purinergic receptors known to be present in PSCs at innervated mature NMJs (Arbour et al., 2015; Rochon et al., 2001). Ca^{2+} responses were elicited by muscarine (20 μM; Figure 1b,c), acetylcholine (ACh; 20 μM; Figure 1d,e) or ATP (20 μM; Figure 1f,g), indicating that PSCs maintained their ability to detect the presence of neurotransmitters even in the sustained absence of innervation. However, muscarine-induced Ca^{2+} responses were significantly reduced at denervated NMJs in comparison to contralateral sham controls (Figure 1b,c; at innervated NMJs: $218.80 \pm 28.50\% \Delta F/F_0$, $N = 7$, $n = 16$ vs. at denervated NMJs: $81.30 \pm 12.10\% \Delta F/F_0$, $N = 7$, $n = 23$; paired t-test, $p < .05$). To compensate for the impossibility to test PSCs responsiveness to endogenous transmitter release due to denervation, we locally applied ACh (20 μM), the natural neurotransmitter in this synapse. Again, ACh induced Ca^{2+} responses in PSCs at denervated NMJs that were significantly smaller that the ones evoked at innervated NMJs (Figure 1d,e; at innervated NMJs: $161.70 \pm 25.50\% \Delta F/F_0$, $N = 7$, $n = 16$ vs. at denervated NMJs: $71.10 \pm 19.80\% \Delta F/F_0$, $N = 4$, $n = 17$; paired t-test, $p < .05$). However, the purinergic activation of PSCs was unchanged (Figure 1f,g; at innervated NMJs: $195.10 \pm 12.00\% \Delta F/F_0$, $N = 7$, $n = 16$ vs at denervated NMJs: $157.00 \pm 36.80\% \Delta F/F_0$, $N = 7$, $n = 23$; paired t-test, $p > .05$). Overall, these results show that, at denervated NMJs, PSCs remain fully potent to detect neurotransmitters but with a decreased muscarinic excitability.

3.2 | mAChRs regulate the expression of the phagocytic marker galectin-3 in PSCs

PSCs acquire macrophage-like behaviors after a nerve injury (Duregotti et al., 2015; Reichert et al., 1994) as indicated by the stable expression of the phagocytic marker galectin-3 (MAC-2), 2 to 5 days after a nerve injury (Martineau et al., 2020). In addition, changes in PSCs gene expression following injury are regulated by mAChRs (Georgiou et al., 1994, 1999). Hence, we posit that changes in mAChRs activation in PSCs following injury regulate the expression of the phagocytic response.

To test this possibility, we performed in vivo intermuscular injections of either saline (0.9%) or muscarine (10 μM) over a 48-hours period following nerve injury. A first injection was performed immediately following the nerve crush injury and every 5 h thereafter (Figure 2a,b). In line with their normal response to denervation (Martineau et al., 2020), the immunofluorescence staining revealed that a large proportion of PSCs robustly expressed galectin-3 48 h after a nerve crush injury in Saline-treated animals (Figure 2c). However, we found that galectin-3 expression in PSCs was significantly reduced in Muscarine-treated animals (Figure 2d; 950.80 ± 51.84 a.u. for the Saline group, $N = 3$, $n = 117$ vs. 690.50 ± 40.00 a.u. for the Muscarine group, $N = 3$, $n = 140$; Mann–Witney test, $U = 5655$, $p < .0001$). These results indicate that galectin-3 expression is regulated by mAChRs activation in PSCs.

3.3 | PSCs mAChRs excitability is not reduced at denervated NMJs in ALS

Next, we investigated whether this reduced muscarinic activation of PSCs was also present at denervated NMJs in a pathological context. Based on the reduced PSCs muscarinic activation at denervated NMJs, one would predict that it should be reduced at denervated NMJs in ALS. However, we previously reported that PSCs at innervated NMJs from SOD1 mice had an early and persistent muscarinic overactivation during the pre-onset stage of the disease in the SOL muscle (Arbour et al., 2015). Moreover, numerous PSCs failed to upregulate galectin-3 on denervated NMJ in this ALS mouse model (Martineau et al., 2020), suggesting that PSCs muscarinic adaptation may be defective at denervated NMJs in ALS.

We analyzed PSCs activation in a model of ALS (SOD1^{G37R}), where adult-onset NMJ denervation is observed (Tremblay et al., 2017). To visualize the state of innervation of all NMJs in situ,

FIGURE 1 Reduced PSC mAChRs activation following NMJ denervation. (a) False color confocal images of two NMJs from an innervated and denervated SOL muscle. Note the presence of the postsynaptic endplate areas (labeled with α-BTX, red) and extensive glial coverage (labeled with S100, cyan). However, note the presynaptic staining (labeled with NF-M + SV2, green) at the innervated NMJ, but not at the denervated one, confirming the absence of presynaptic innervation (white arrow). (b, d, f) Ca^{2+} responses in PSCs of denervated (red trace) and sham operated NMJs (black trace) elicited by local application of muscarine (20 μM) (b), ACh (20 μM) (d), and ATP (20 μM) (f) Note that ATP-induced Ca^{2+} responses in PSCs remained unchanged following denervation while muscarine and ACh were significantly reduced. Histograms in (c), (e) and (g) represent mean ± SEM of PSC Ca^{2+} responses elicited by local application of muscarine, ACh and ATP respectively at sham operated (innervated; black) and denervated (red) NMJs. Scale bars = 10 μm. *$p < .05$. NMJ, neuromuscular junction; PSC, perisynaptic Schwann cell.
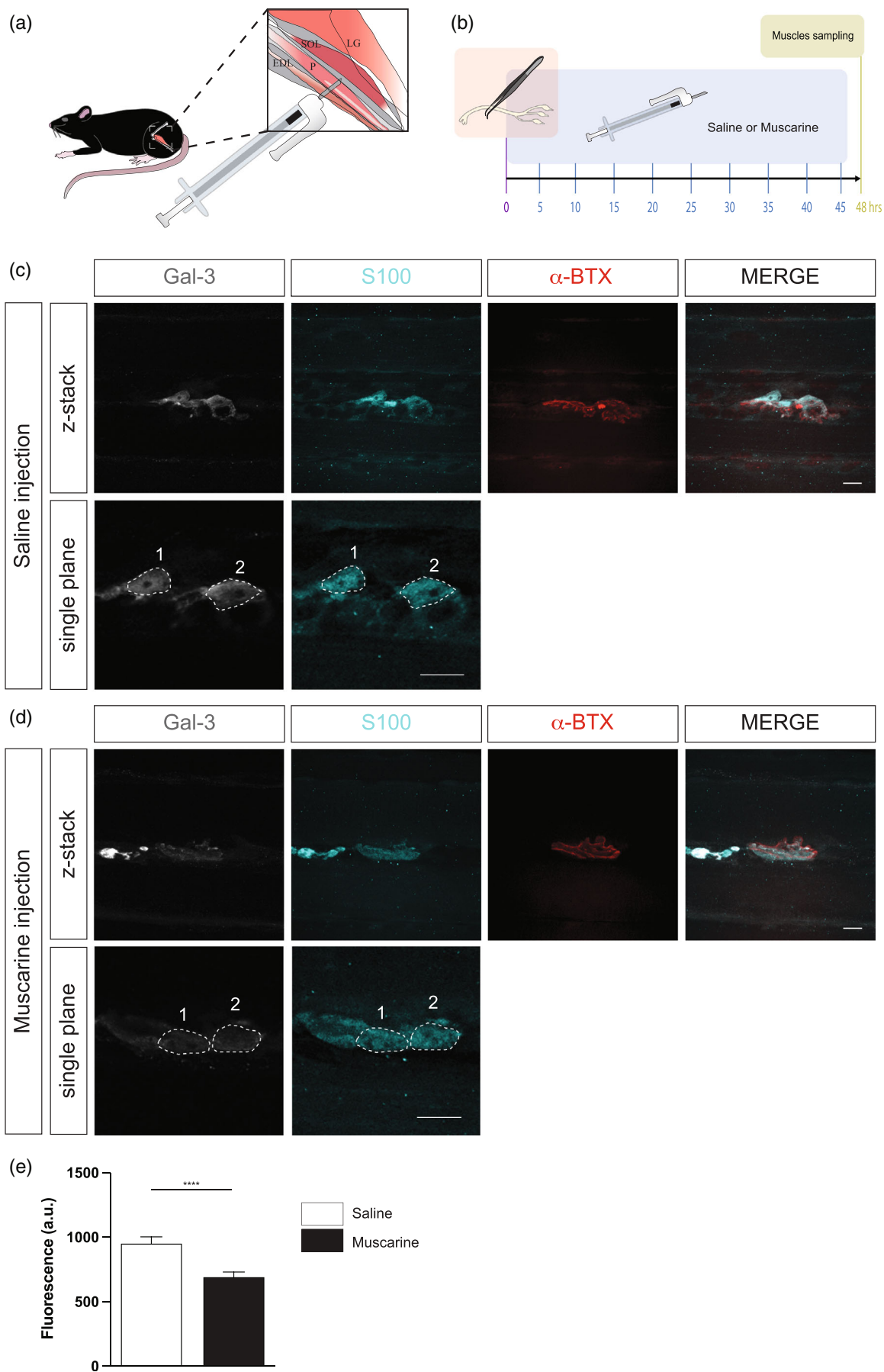
FIGURE 2 Legend on next page.

we crossed them with Thy1-YFP to generate YFP.SOD1^{G37R} mice which expressed YFP in all MNs and nerve terminals (Feng et al., 2000). All mice developed a motor neuron disease with motor symptoms similar to the human ALS disease and the SOD1^{G37R} mice (data not shown) albeit with shifted disease onset and duration (see Section 2 for details; Martineau et al., 2020; Tremblay et al., 2017). In every case, the status of innervation was further confirmed using either electrophysiological recordings of synaptic events and/or by immunolabeling of synaptic elements of the same recorded NMJs, as previously described (Arbour et al., 2015; Tremblay et al., 2017). This combination of methods greatly limit confounding factors such as partially innervated NMJ into the analysis. For instance, an NMJ would have been categorized as denervated with the YFP signal (Figure 3a), yet the amplitude of the EPP generated was similar to the neighboring innervated NMJ (Figure 3b) while the immunofluorescence staining revealed only a small (~10%) remnant of presynaptic coverage of the NMJ (Figure 3c). This set of experiments suggests that a careful investigation and categorization should be performed at NMJs by using more than one method. Hence, all NMJs identified as denervated, based on the lack of YFP fluorescent signal at identified endplates labeled with α-BTX (Figure 3d), also failed to show any sign of synaptic activity (spontaneous nor evoked; Figure 3e) and/or pre-synaptic staining (Figure 3f).

Ca^{2+} responses were elicited by local application of muscarine (10 μM) on PSCs at denervated NMJs. Unlike the reduced PSCs muscarinic activation observed at denervated NMJs, we found no statistical difference between the amplitude of Ca^{2+} responses evoked in PSCs associated with denervated and innervated NMJs in this ALS model (Figure 3g; at innervated NMJs: 347.1 ± 54.6% $\Delta F/F_0$, $N = 6$, $n = 10$ vs. at denervated NMJs: 316.9 ± 46.7% $\Delta F/F_0$, $N = 5$, $n = 8$; unpaired t-test, $p = .6890$). Then, we analyzed PSC Ca^{2+} responses evoked by local application of ATP (10 μM) on the same PSCs. Surprisingly, amplitudes of PSC Ca^{2+} responses were reduced by 28% at denervated NMJs in the YFP.SOD1^{G37R} mice (Figure 3h; at innervated NMJs: 655.9 ± 31.84% $\Delta F/F_0$ vs at denervated NMJs: 470.6 ± 65.13% $\Delta F/F_0$; unpaired t-test, $p = .0150$). Hence, these data suggest that muscarinic and purinergic PSCs activation do not develop the proper phenotype expected for NMJ repair following denervation in this ALS mouse model.

Overall, at denervated NMJs, mAChR-driven activation of PSC was reduced and this downregulation modified PSC galectin-3 expression. This reduced muscarinic activation was not observed at denervated NMJs in a SOD1 mouse model of ALS.

We then addressed our second goal and investigated PSC properties during NMJ reinnervation.

3.4 | Reduced PSC mAChRs contribution to synaptic transmission at immature NMJs

The reinnervation process is thought to recapitulate in part the events that take place during NMJ formation and maturation during development (Darabid et al., 2014; Rich & Lichtman, 1989). Interestingly, PSC mAChRs and purinergic receptors are already present and functional as early as P7-8 (Darabid et al., 2013; Heredia et al., 2018). In addition, while only PSCs purinergic receptors significantly contribute to neurotransmission detection at P7-8 NMJs (Darabid et al., 2013; Heredia et al., 2018), both mAChRs and purinergic receptors contribute at adult NMJs (Rochon et al., 2001). However, when these functional properties appear and how they evolve along the developmental process remain unclear, making predictions difficult for the PSC properties during reinnervation.

We examined PSCs activation by muscarinic and purinergic receptors at different postnatal ages (P3, P7, P14 and P21). These ages encompass the main steps observed during reinnervation, from extended polyinnervation and synaptic competition (P3) to complete monoinnervation (P21) (Balice-Gordon & Lichtman, 1993; Hirata et al., 1997).

We first analyzed PSCs Ca^{2+} responses elicited by the release of neurotransmitter, upon motor nerve stimulation (50 Hz, 30 s; activation of synaptic receptors), at the different ages in control and in the presence or absence of the general muscarinic antagonist atropine (20 μM). Motor nerve stimulation elicited Ca^{2+} responses in PSCs at all ages and stages of postnatal NMJ maturation, in the presence or absence of atropine (Figure 4a). However, the effect of atropine on the amplitude of PSCs Ca^{2+} responses was more pronounced as NMJs developed to more mature states (at P3 without atropine: 107.00 ± 10.84%$\Delta F/F_0$, $N = 4$, $n = 5$; at P3 with atropine: 89.05 ± 18.83%$\Delta F/F_0$, $N = 5$, $n = 6$; at P7 without atropine: 65.87 ± 14.04%$\Delta F/F_0$, $N = 5$, $n = 9$; at P7 with atropine: 41.04 ± 13.83%$\Delta F/F_0$, $N = 4$, $n = 7$; at P14 without atropine: 52.40 ± 10.21%$\Delta F/F_0$, $N = 5$, $n = 10$; at P14 with atropine: 22.54 ± 11.13%$\Delta F/F_0$, $N = 4$, $n = 7$; at P21 without atropine: 41.72 ± 7.00%$\Delta F/F_0$, $N = 5$, $n = 9$; at P21 with atropine: 11.82 ± 4.45%$\Delta F/F_0$, $N = 4$, $n = 5$; One-way ANOVA; $F_{(3,19)} = 5.287$; $p = .0081$). Notably, in the presence of atropine, the normalized PSCs Ca^{2+} responses from P3 NMJs were significantly larger than responses from P14 and P21 NMJs (Tukey's multiple comparison post hoc test; P3 vs. P14, $p < .01$; P3 vs. P21, $p < .05$). This indicates that PSCs mAChR contribution was minimal at P3 and increased with developmental age, representing a fourfold increase (up to 72% in P21 mice in comparison to 17% in P3 animals;

FIGURE 2 mAChRs activation reduces galectin-3 expression in PSCs at denervated NMJs. (a) Schematic representation of the intermuscular injection between the *peroneus* (P) and the *lateral gastrocnemius* (LG) muscles to target the SOL. (b) Timeline of the nerve crush injury (time 0, red square, diagram of nerve crush), the repeated intermuscular injections (bleu rectangle), and the endpoint, where muscles were collected for immunofluorescence processing (green square). (c, d) False color confocal images of a z-stack (low magnification) and a single plane (high magnification) focusing on one NMJ with two PSCs (S100, cyan) caping the nAChRs (α-BTX, red) and expressing galectin-3 (Gal-3, gray) of a Saline-injected animal (c) and a Muscarine-injected animal (d). Note the Gal-3 staining within the PSCs soma and the brightest intensity in the Saline-injected animal compared to the Muscarine-injected animal. (e) Histogram showing the mean ± SEM of arbitrary unit value of the Gal-3 staining analysis of the two groups. Scale bars = 10 μm. ****$p < .0001$. NMJ, neuromuscular junction; PSC, perisynaptic Schwann cell.
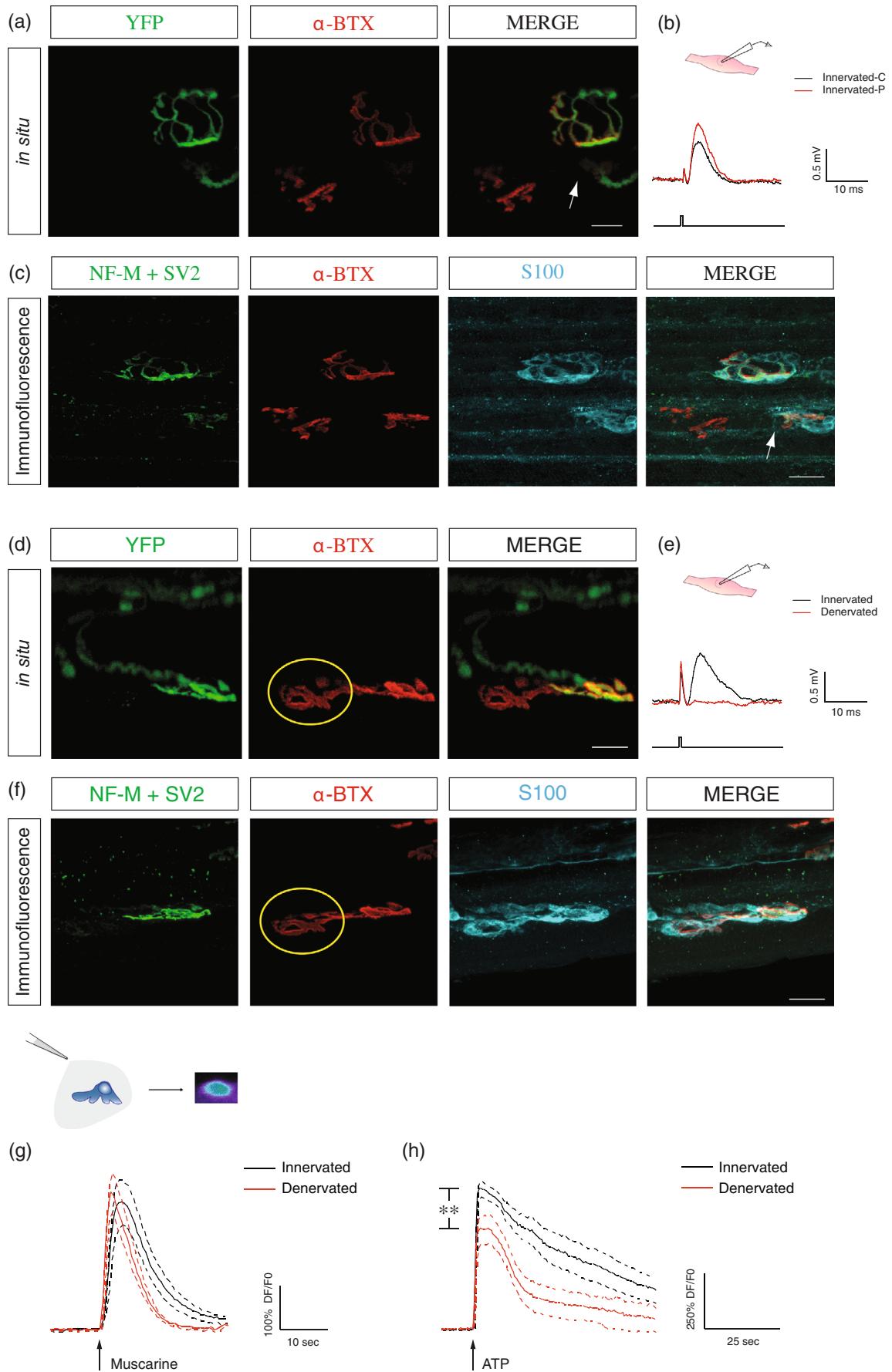
FIGURE 3 Legend on next page.

represented as blue rectangles in Figure 4b). Our results are consistent with those in early postnatal stages of NMJ development and those at adult monoinnervated NMJs.

Importantly, local applications of muscarine (Figure 4c) and ATP (Figure 4d) revealed that both types of receptors are present and functional at all ages tested during development. PSC responses to local application of muscarine (10 μM) were not significantly different at different ages (Figure 4c; values for P3, P7, P14 and P21 were respectively 4.53 ± 1.57%$\Delta F/F_0$ ($N = 3$, $n = 12$), 8.61 ± 2.56%$\Delta F/F_0$ ($N = 3$, $n = 20$), 4.28 ± 1.6%$\Delta F/F_0$ ($N = 2$, $n = 23$), and 7.05 ± 1.46%$\Delta F/F_0$ ($N = 2$, $n = 28$); One-way ANOVA; $F_{(3,79)} = 1.17$; $p = .3264$). However, Ca^{2+} responses elicited by ATP application (10 μM) were different only at P14 (Figure 4d; (Tukey's multiple comparison post hoc test; P3 vs. P14, $p < .05$; P7 vs. P14, $p < .001$; P14 vs. P21, $p < .01$). Values from P3, P7, P14 and P21 groups were respectively 35.60 ± 3.11%$\Delta F/F_0$ ($N = 3$, $n = 23$), 42.94 ± 2.86%$\Delta F/F_0$ ($N = 3$, $n = 28$), 24.21 ± 1.82%$\Delta F/F_0$ ($N = 2$, $n = 33$) and 35.55 ± 2.55%$\Delta F/F_0$ ($N = 2$, $n = 51$); One-way ANOVA; $F_{(3,131)} = 7.793$; $p < .0001$). In summary, these results suggest that PSCs functional properties evolve during the NMJ maturation process, and a reduced muscarinic contribution is observed at immature NMJs.

3.5 | High morphological and physiological plasticity during reinnervation

We asked how PSCs excitability changed during the reinnervation process. If reinnervation recapitulates NMJ maturation, we should anticipate a reduced muscarinic contribution during synaptic communication (upon nerve stimulation), without changes in PSC mAChRs or purinergic receptors activation, at reinnervating NMJs. Sciatic nerve was crushed to induce denervation and allow subsequent reinnervation. We first determined the time window best suited to study PSCs, by determining the time course of the denervation and reinnervation using immunolabeling and electrophysiological recordings.

Denervation was confirmed by the lack of colocalization of the pre- and postsynaptic staining (Figure 5a) and of muscle contractions

and endplate potentials (EPPs) at 7 DPI (Figure 5b), even when the motor nerve was stimulated with suprathreshold intensities (up to four times larger than the ones used in control preparations). Muscle contractions and synaptic responses could be evoked in all nerve-muscle preparations in sham-operated animals (Figure 5b).

During reinnervation, NMJs were categorized as denervated, partially innervated or fully innervated and innervation status was determined (monoinnervated or polyinnervated; Figure 6a–c). NMJ denervation was highest at 8 DPI compared to sham and all other DPI time points (Figure 6c; NMJs denervated: 84.20% ± 6.30%; NMJs innervated: 15.70% ± 6.30%, 8 DPI: $N = 4$, $n = 136$; Sham: $N = 4$, $n = 91$; Sidak post-test, $p < .001$). Complete reinnervation at NMJs became significant at 18 DPI compared to all other DPI (Figure 6c; NMJs denervated: 1.80% ± 1.80%; NMJs innervated: 98.20% ± 1.80%, $N = 3$, $n = 85$; Sidak post-test, $p < .001$). Partial innervation of NMJs was observed at all DPI and was always significantly increased compared to Sham animals (Figure 6a,c; Sidak post-test, 8 DPI: $p = .005$; 10, 12, 14 16 and 18 DPI: $p < .001$). High levels of polyinnervated NMJs were observed at 10 DPI ($N = 4$, $n = 98$) and 12 DPI ($N = 3$, $n = 88$), peaking between 14 DPI (Figure 6a,b; polyinnervated NMJs: 65.80% ± 2.20%; monoinnervated NMJs: 34.20 ± 2.20 $N = 4$ $n = 105$) and 16 DPI (polyinnervated NMJs: 54.80% ± 8.20%; monoinnervated NMJs: 45.20 ± 8.20, $N = 3$ $n = 75$), which were significantly different from sham animals, 8 and 18 DPI animals (Sidak post-test, $p < .001$). Interestingly, PSC process extension and nerve terminal sprouting were mostly observed during that period. Hence, it appears that the time window between 14 and 16 DPI is the highest plasticity period as revealed by a high morphological plasticity and reorganization. Furthermore, percentage of polyinnervated NMJ drastically dropped after 16 DPI and preparations were physiologically stable (see Section 2), thus facilitating functional analyses.

We next tested the synaptic competence of polyinnervated NMJs using the ventral root-muscle preparations to stimulate independently the nerve terminals innervating a polyinnervated NMJ and perform electrophysiological recordings of EPPs. As shown in Figure 6d, upon independent ventral root stimulation, synaptic responses were elicited

FIGURE 3 PSC mAChRs activation is not reduced at denervated NMJs in YFP.SOD1^{G37R} animals. (a) False color confocal images of two NMJs from an YFP.SOD1^{G37R} animal (P460), expressing yellow fluorescent protein (YFP) in all motor axons and nerve terminals (green). During the in situ Ca^{2+} imaging experiment, postsynaptic nAChRs were labeled with α-bungarotoxin (α-BTX, red) to discriminate between innervated and denervated NMJs. Note the small partially innervated area (arrow) of the NMJ at the bottom. (b) The amplitude of the EPP (nerve stimulation, lower trace) at the partially innervated NMJ (Innervated-P, red trace) was comparable to the one generated by a nearby completely innervated NMJ (Innervated-C; black trace). (c) Immunohistochemical staining of the same two NMJs shown in (a) with two presynaptic markers (NF-M+ SV2, green) to further confirm the state of innervation. PSCs were labeled using S100 antibody (cyan). (d) False color confocal images of two NMJs from another YFP.SOD1^{G37R} animal (P460), expressing YFP (green). Postsynaptic nAChRs were labeled with α-bungarotoxin (α-BTX, red) during the Ca^{2+} imaging experiments. Note that the NMJ on the left (yellow circle) was denervated as indicated by the absence of the YFP signal over the α-BTX staining. (e) Lack of evoked EPP (nerve stimulation, lower trace) at this denervated NMJ (red trace) while EPPs were evoked at the neighboring innervated NMJ (black trace). (f) Immunohistochemical staining of the same two NMJs shown in (d) was performed with two presynaptic markers (NF-M+ SV2, green) to further confirm the state of innervation. PSCs were labeled using S100 antibody (cyan). (g) Mean PSC Ca^{2+} responses (solid line) ± SEM (dotted lines) induced by local application of muscarine (10 μM) in PSCs associated with innervated (black traces) or denervated (red traces) NMJs. No significant difference was observed between the amplitude of Ca^{2+} responses. (h) Similar experiments on the same cells but with local applications of ATP (10 μM). Note ATP-elicited responses were smaller at denervated NMJs. Scale bars = 20 μM. **$p < .01$. NMJ, neuromuscular junction; PSC, perisynaptic Schwann cell.
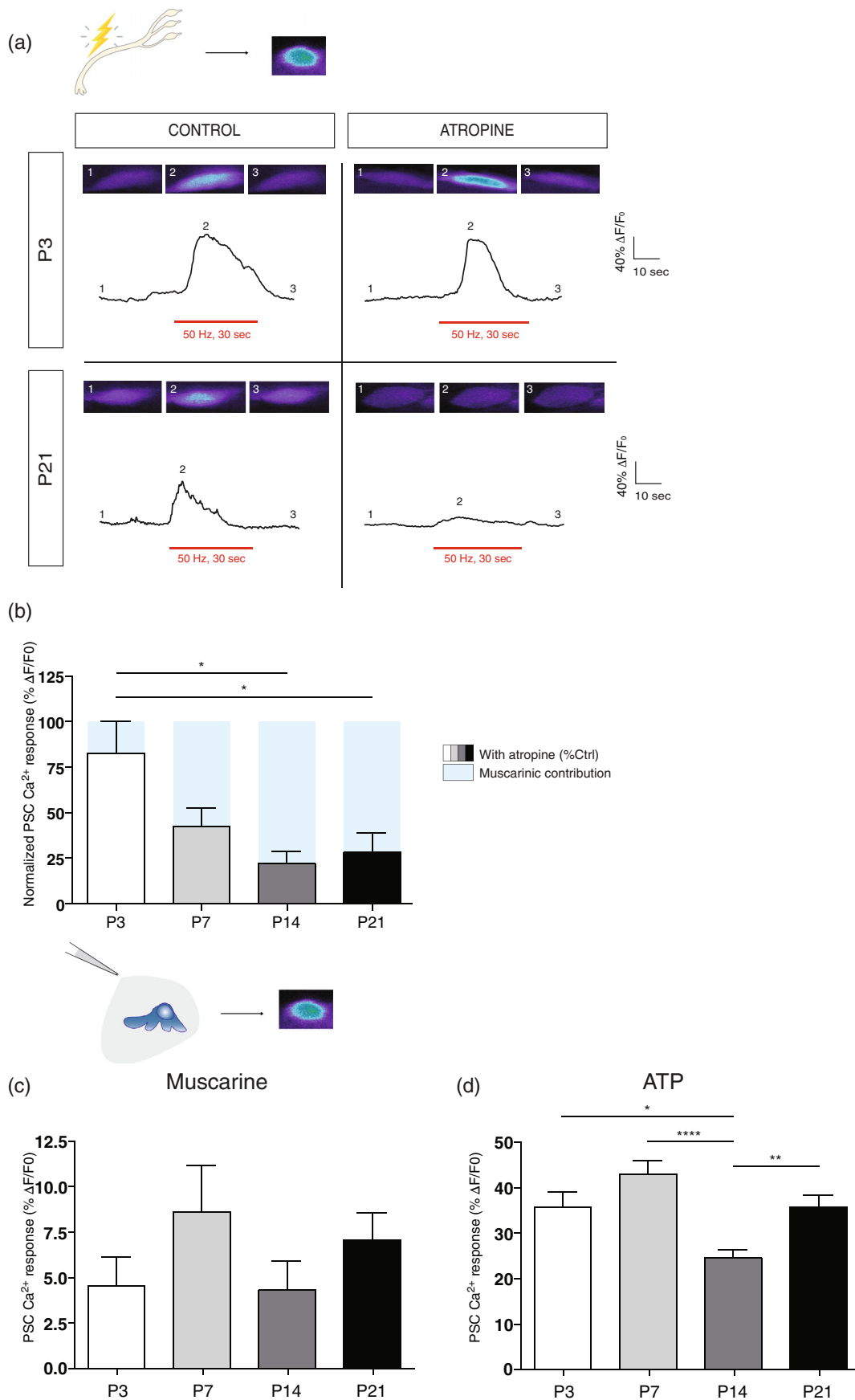
FIGURE 4 Legend on next page.

by each nerve terminal innervating a given NMJ. This shows that the competing nerve terminals at the same NMJ were functional during the process of reinnervation following injury.

During development, synaptic strength heterogeneity was reported at polyinnervated NMJs (Darabid et al., 2013; Darabid et al., 2018), reflecting the different status of ongoing synaptic competition. We examined this possibility by comparing synaptic responses of the competing nerve terminals at polyinnervated NMJs during the reinnervation period (between 14 and 16 DPI). As shown in Figure 6d, consistent with ongoing synaptic competition, independent and selective ventral root stimulation evoked different relative EPP amplitude generated by the two competing nerve terminals at the same NMJ ($N = 6$, $n = 6$).

Finally, during postnatal development, competing nerve terminals with distinct synaptic strength generate different forms of synaptic plasticity elicited by high frequency motor nerve stimulation (HSF; 50 Hz, 30 s; Figure 6e; Darabid et al., 2018). This was also observed at polyinnervated NMJs following reinnervation where nerve terminals with the largest quantal content produced only a short-term potentiation (Figure 6f; Strong terminals: $N = 11$, $n = 11$; EPP amplitude of $99.78 \pm 0.58\%$ during baseline vs. $116.90 \pm 4.26\%$ 5 min post-HFS vs. $98.96 \pm 2.32\%$ 20 min post-HFS; One-way ANOVA; $F_{(2,30)} = 12.94$; $p < .0001$) while nerve terminals with the smallest quantal content produced a short-term potentiation and long-term depression (Figure 6g; Weak terminals: $N = 10$, $n = 10$; EPP amplitude of $99.21 \pm 0.50\%$ during baseline vs. $108.00 \pm 4.55\%$ 5 min post-HFS vs. $85.17 \pm 3.88\%$ 20 min post-HFS; One-way ANOVA; $F_{(2,27)} = 11.09$; $p = .0003$).

These results suggest that synaptic properties during reinnervation are reminiscent of those observed during NMJ postnatal maturation. Hence, we next investigated whether PSCs functional properties also reproduce their properties during this period of high demand of morphological and physiological plasticity (between 14 and 16 DPI).

3.6 | Reduced PSC mAChRs contribution at reinnervating NMJs

We investigated mAChRs contribution to PSCs activation elicited by synaptic transmission at reinnervating NMJs. No data from denervated NMJs were included and mono- and polyinnervated NMJs were selected and are hereafter referred as «reinnervating NMJs».

We tested if PSCs at reinnervating NMJs can detect endogenous release of neurotransmitter and, if so, what was the mAChRs contribution. We used the same motor nerve stimulation regime (50 Hz, 30 s) and simultaneously monitored PSC Ca^{2+} responses in the presence or absence of atropine (20 μM). The motor nerve stimulation elicited Ca^{2+} elevation in control and in reinnervating NMJs and were reduced in the presence of atropine (Figure 7a). To determine the mAChRs contribution at reinnervating NMJs, we compared the normalized PSC Ca^{2+} responses in the presence of atropine relative to control. As shown in Figure 7b, the muscarinic contribution was significantly smaller at PSCs of reinnervating NMJs than the one at Sham NMJs (67% of in sham vs. 38% in reinnervating; sham w/o atropine: $54.10 \pm 12.35\%\Delta F/F_0$, $N = 5$, $n = 6$; sham + atropine: $18.06 \pm 4.98\%\Delta F/F_0$, $N = 4$, $n = 6$; reinnervating w/o atropine: $123.26 \pm 25.49\%\Delta F/F_0$, $N = 5$, $n = 8$; reinnervating + atropine: $81.89 \pm 12.54\%\Delta F/F_0$, $N = 9$, $n = 15$; unpaired t-test, $p = .0486$). As predicted, PSC Ca^{2+} responses were more reduced by atropine at sham NMJs than reinnervating ones (67% of contribution to synaptic transmission in sham vs. 38% in reinnervating).

While the type of purinergic receptors regulating synaptic communication remains elusive at adult NMJs (Arbour et al., 2015; Rochon et al., 2001), they rely on P2Y1 receptors during development (Darabid et al., 2013, 2018). Hence, since our results show similar properties in development and reinnervation (Figures 6 and 7), we tested the selective P2Y1 antagonist, MRS 2179, known to block all purinergic components during development (Darabid et al., 2013, 2018). However, PSC Ca^{2+} responses evoked by ATP were not totally blocked by MRS 7179, neither by the combination of MRS 2179 and a selective A1 antagonist, DPCPX (data not shown–reduction of 64%), preventing further investigation of the endogenous purinergic contribution. In summary, the cholinergic contribution was reduced at reinnervating NMJs as was reported during postnatal NMJ maturation process.

3.7 | Reduced muscarinic and purinergic activation of PSCs at reinnervating NMJs

To further characterize PSC properties at reinnervating NMJs, we investigated their responsiveness to local exogenous activation of mAChRs and purinergic receptors. This approach was useful to determine the maturation of PSC properties during postnatal NMJ development (Figure 4).

FIGURE 4 Changes of PSC mAChRs contribution during NMJ formation and maturation. (a) Representative PSC Ca^{2+} responses elicited by motor nerve stimulation (red bar; 50 Hz, 30 s) from P3 (top) and P21 mice (bottom), in the absence (left) and presence (right) of atropine (20 μM). Insets show representative confocal images of the Ca^{2+} level in PSCs loaded with the Ca^{2+} indicator Fluo4 AM before (1), at the peak of the response (2) and after (3) the stimulation. Note that atropine greatly reduced Ca^{2+} responses of PSCs from P21 mice but had no effect on the ones from P3 pups. (b) Histograms showing the normalized PSC Ca^{2+} responses in the presence of atropine relative to control. Note that the mAChRs contribution (blue) is significantly smaller at developmental ages of P3 (white) and P7 (light gray) compared to P14 (dark gray) and P21 (black) respectively. (c) Histogram showing the mean ± SEM of PSC Ca^{2+} responses elicited by local application of muscarine (10 μm) and (d) ATP (10 μm) at different postnatal ages (P3; white, 7; light gray, 14; dark gray, 21; black). $*p < .05$, $**p < .01$, $***p < .005$. NMJ, neuromuscular junction; PSC, perisynaptic Schwann cell.
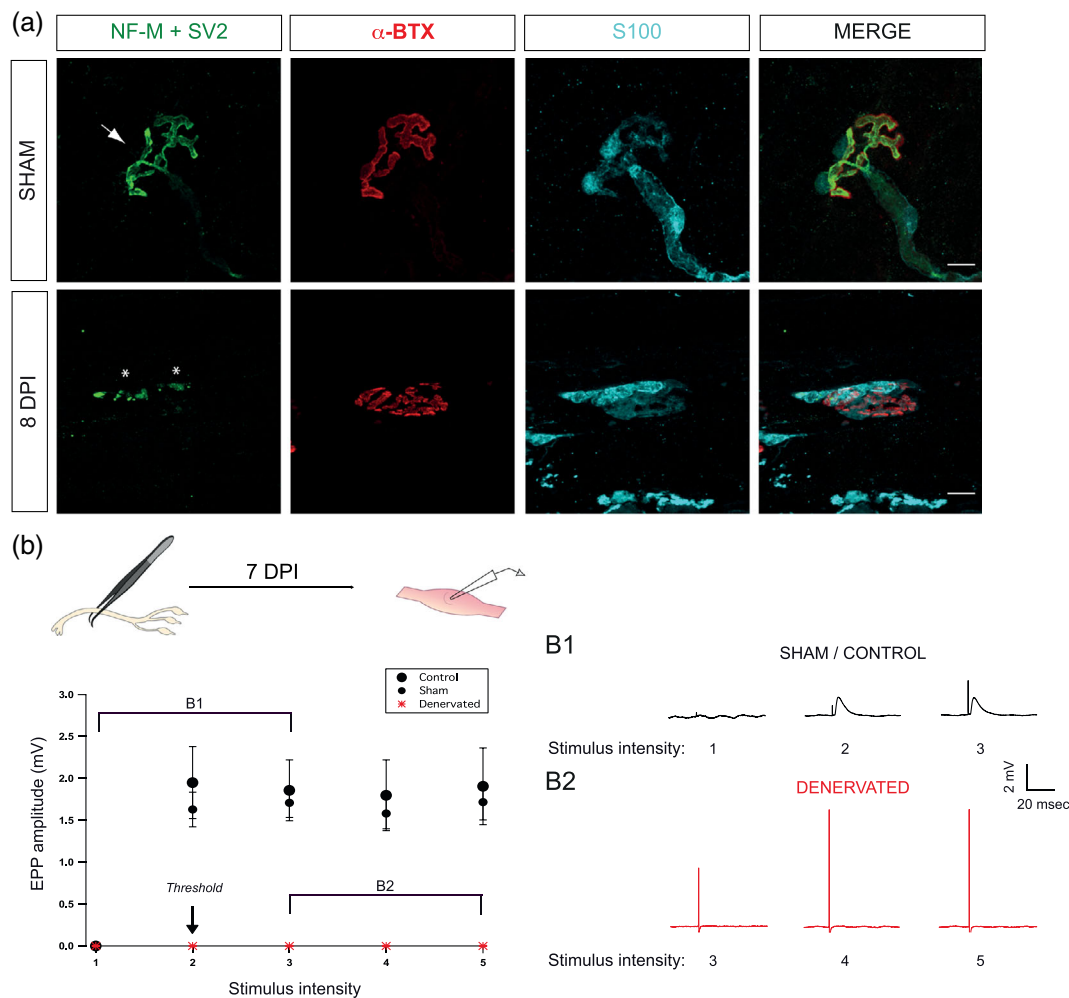
FIGURE 5 Morphological and functional denervation prior reinnervation. (a) Confocal images of a NMJ from a SOL Sham and 8 days post-injury (DPI) animals. Muscles were labeled for the nerve terminals (NF-M + SV2, green), postsynaptic nAChRs (α-BTX, red) and Schwann cells (S100, cyan). In Sham operated animals, nicotinic receptors in the muscle endplate are completely covered by a single nerve terminal (arrow) while at 8 DPI animals, NMJ were mostly denervated, as indicated by the absence of the presynaptic staining over the α-BTX signal. Note the presence of axonal debris in the 8 DPI animals (asterisks). (b) Denervation was confirmed using synaptic recordings. Graph showing the average EPP amplitude (mV) at different intensity of motor nerve stimulation from control (●), sham (●), and denervated muscles (red *). The five points of the X axis represent different intensity of stimulation, 1 being a subthreshold stimulation, 2 the threshold intensity applied to induce contraction, and 3, 4, and 5, doubling the intensity of the preceding value. (b1) Representative traces showing EPP evoked at an NMJ from a control muscle and (b2) a denervated one. Note the increased size of the artifact of stimulation reflecting the increased intensity of stimulation. Scale bars: 10 μm. EPP, endplate potential; NMJ, neuromuscular junction.

We used mice expressing yellow fluorescent protein (YFP) in all motor neurons (MNs) and MN nerve terminals (Feng et al., 2000) to visualize the presence of axons at the reinnervating NMJs, 14 and 16 DPI. The presence of axons was further confirmed by immunolabeling performed post-experiment as previously described (Arbour et al., 2015; Tremblay et al., 2017).

Ca^{2+} responses induced by local application of muscarine (10 μM) were significantly smaller at reinnervating NMJs (Figure 8a; sham: 340.70 ± 30.23%$\Delta F/F_0$, $N = 4$, $n = 25$; reinnervating: 202.50 ± 25.57%$\Delta F/F_0$, $N = 5$, $n = 25$; unpaired t-test, $p = .0011$). Similar to muscarine, ATP (10 μM) induced Ca^{2+} responses were significantly smaller at reinnervating NMJs (Figure 8b; sham: 409.40 ± 24.41%$\Delta F/F_0$, $N = 4$, $n = 36$; reinnervating, 175.40 ± 21.97%$\Delta F/F_0$, $N = 5$, $n = 22$; unpaired t-test, $p < .0001$). Interestingly, when

the same PSCs were activated by the sequential local application of both agonists, there was a positive linear correlation between the amplitude of Ca^{2+} responses evoked by muscarine and ATP (Figure 8c; $N = 5$, $n = 18$; $r(16) = 0.6987$, $p = .0013$; Figure 8c1, c2), while no correlation was observed at NMJs from Sham-operated mice (data not shown; $N = 4$, $n = 24$; $r(22) = 0.1487$, $p < .05$). This linear correlation of PSC Ca^{2+} responses highlights a novel coherence between the two families of receptors at reinnervating NMJs.

Together, these results suggest that the muscarinic and purinergic recruitments of PSC synaptic and extrasynaptic receptors are reduced in a synaptic context of reinnervation. Therefore, during the reinnervation process, PSCs seem to have a different profile of properties than denervation and development.
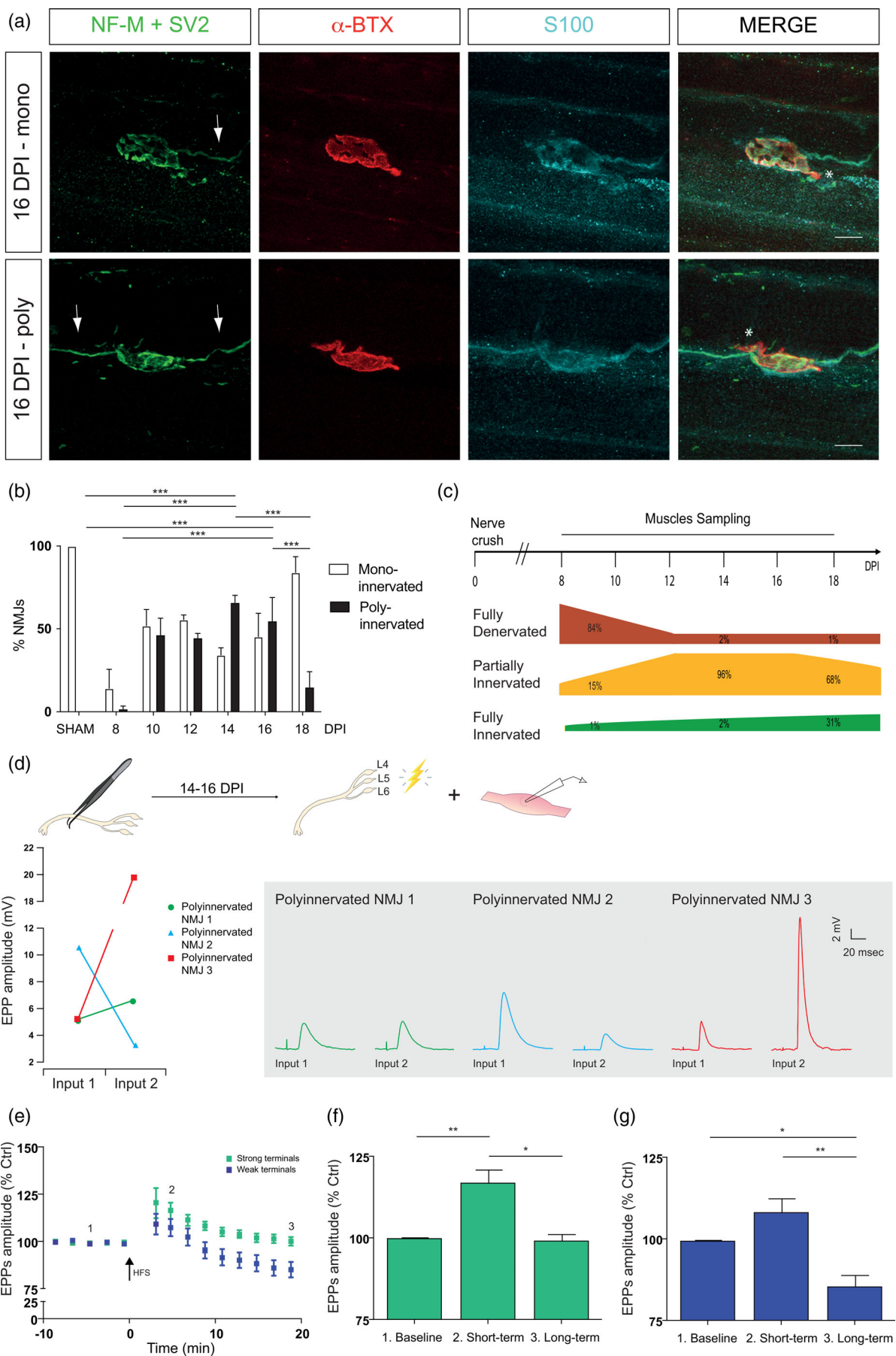
FIGURE 6 Legend on next page.

3.8 | Amplitudes of PSCs Ca^{2+} responses are not correlated with the number of axon(s) and PSC process(es) extension at reinnervating NMJs

We further explored changes to the PSC phenotype during reinnervation. PSCs undergo morphological changes during NMJ repair or after a pharmacological manipulating of their muscarinic signaling (Wright et al., 2009). Also, they can detect multiple nerve terminals at the same NMJ (Darabid et al., 2013) and adapt their functional properties according to the level of synaptic activity (Belair et al., 2010; Rousse et al., 2010). Hence, we tested whether the functional state could be correlated with morphological signs of repair (PSC process extensions, polyinnervation). To test this possibility, we correlated the amplitude of PSC Ca^{2+} responses evoked by muscarine and ATP with the number of axon(s) and PSC process(es) extension.

During in situ Ca^{2+} imaging experiments, PSCs localisation onto the postsynaptic area (α-BTX staining) was determined (Figure 9a—upper panel) and the amplitude of their Ca^{2+} responses evoked by muscarine and ATP recorded (Figure 9a—middle panel). The number of innervating axon(s) was determined using the YFP signal (Figure 9a—lower panel) and subsequently confirmed with the immunolabeling of the presynaptic staining (data not shown). The immunofluorescence against a presynaptic (not shown) and glial marker (S100) combined with the α-BTX staining was performed after the Ca^{2+} imaging experiment and allowed us to identify the presence of process extension from the same PSC (Figure 9b).

Figure 9a,b shows a PSC eliciting Ca^{2+} responses with small amplitude upon local applications of muscarine and ATP at a mono-innervated NMJ (1 axon) and the presence of a process extension. We further evaluated the correlations using a Spearman's rank correlation coefficient. No correlation was observed between the peak of PSC Ca^{2+} responses elicited by muscarine and the number of axon(s), nor with the number of PSCs process(es) extension (Figure 9c; $N = 5$, $n = 17$, max peak muscarine vs. axon, $r(15) = 0.09$, $p < .05$; max peak

muscarine vs. process extension, $r(15) = -0.33$, $p < .05$; axon vs. process extension, $r(15) = 0.28$, $p < .05$). Similarly, no correlation was found when comparing to the max peak of the PSC in response to ATP (Figure 9d; $N = 5$, $n = 13$, max peak ATP vs. axon, $r(11) = 0.47$, $p < .05$; max peak ATP vs. process extension, $r(11) = 0.29$, $p < .05$; axon vs. process extension, $r(11) = -0.08$, $p < .05$).

3.9 | Extended period of changed PSC properties following reinnervation

Finally, we determined the period of changed PSC properties following reinnervation. Using the same experimental strategy to induce denervation and subsequent reinnervation, PSC mAChRs and purinergic receptors activation was investigated 60 and 90 DPI. NMJs studied for in situ Ca^{2+} imaging experiments were later retrieved following the immunolabeling process, and the innervation status was determined and correlated with the YFP signal (data not shown). As expected, the vast majority of NMJs were monoinnervated after 60 and 90 DPI (81% and 95%, respectively; Figure 10a).

Interestingly, PSC Ca^{2+} responses evoked by muscarine (10 μM) were still reduced at 60 DPI compared to control (One-way ANOVA Kruskal–Wallis test, $p = .0138$; Figure 10b,d). This is more than 30 days after complete reinnervation following nerve injury. We then investigated PSCs properties 90 DPI and found that the PSC properties were now similar to control. Values for controls, 60 and 90 DPI were respectively 283.40 ± 31.12%$\Delta F/F_0$ ($N = 7$, $n = 34$), 159.20 ± 36.91%$\Delta F/F_0$ ($N = 4$, $n = 20$), and 301.30 ± 38.48%$\Delta F/F_0$ ($N = 3$, $n = 16$; Dunn's multiple-comparison post-test; Not injured vs. 60 DPI, $p = .0256$; 60 DPI vs. 90 DPI, $p = .0391$; Not injured vs. 90 DPI, $p > .05$). Concerning ATP activation, there was no statistical difference among the groups in PSC Ca^{2+} responses elicited by the local application of ATP (10 μM; Figure 10c,e; Kruskal–Wallis test, $p < .05$). The values for controls, 60 DPI and 90 DPI were respectively 535.90

FIGURE 6 Morphological and physiological characterization of reinnervating NMJs. (a) False color confocal images of mono- (top, one axon, arrow) and polyinnervated (bottom, two axons, arrows) NMJs from 16 DPI animals. SOL NMJs were labeled for the nerve terminals (NF-M + SV2, green), postsynaptic nAChRs (α-BTX, red), and Schwann cells (S100, cyan). Note the presence of a partially innervated NMJ (asterisks). (b) Histogram representing the mean percentage ± SEM of mono- (white bars) and polyinnervated (black bars) NMJs. Note that more than half of NMJs were partially innervated with multiple axons between 14 and 16 DPI, suggesting a specific time window of high morphological reorganization. More specifically, at 14 and 16 DPI, the percentage of polyinnervated is the highest in comparison to the percentage of monoinnervated innervation. (c) Schematic representation of the morphological assessment of NMJs from SOL after a sciatic nerve crush injury. Injury was performed at time 0 (nerve crush) and mice were sacrificed at 8, 10, 12, 14, 16 and 18 DPI for NMJ morphological analysis (Muscle sampling). End-plate innervation of NMJs were characterized as either fully denervated (green), partially innervated (yellow) or fully innervated (red) NMJs. (d) Average EPP amplitudes of the two competing nerve terminals of three different polyinnervated NMJs (red, blue and green). The graph shows the large variability in EPP amplitude at individual polyinnervated NMJs, 2 weeks following nerve crush. Right insets illustrate representative EPPs for the competing nerve terminals at the three polyinnervated NMJs elicited by selective ventral root stimulations. (e) Normalized EPP amplitude ± SEM before, during and after high frequency motor nerve stimulation (HFS; 50 Hz, 30 s; black arrow) of strong (green) and weak (blue) terminals. HFS induced a short-term potentiation (2, at 5 min post-HFS) at both terminals but a long-term depression (3, at 20 min post-HFS) only of the weak terminals in comparison to the baseline (1). (f) Histograms showing the mean amplitude of EPPs ± SEM induced by strong and weak (g) terminals during the baseline, shortly after the HFS (short term; at 5 min post-HFS) and 20 min post-HFS (long term). Scale bars: 10 μm. *$p < .05$, **$p < .01$, ***$p < .005$. EPP, endplate potential; HFS, high frequency stimulation; NMJ, neuromuscular junction.
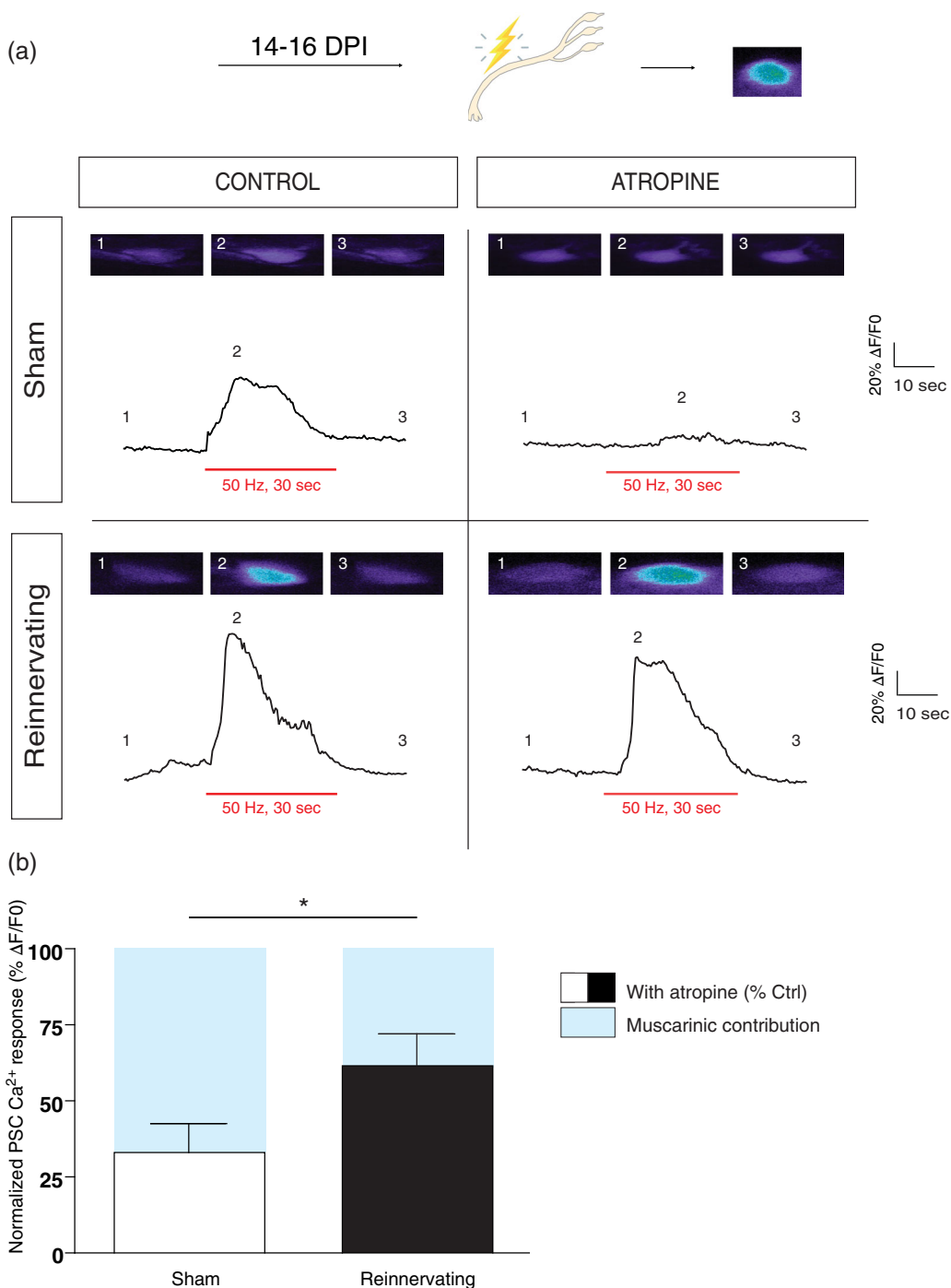
FIGURE 7 Reduced PSC mAChRs contribution at reinnervating NMJs. (a) Representative PSC Ca^{2+} responses elicited by motor nerve stimulation (red bars; 50 Hz, 30 s) from Sham (top) and Reinnervating (bottom) muscles, in the absence (left) and presence (right) of atropine (20 μM). Insets are false color confocal images of the Ca^{2+} level in PSCs loaded with the Ca^{2+} indicator Fluo4 AM before (1), at the peak of the response (2) and after (3) the stimulation. Note that atropine had no significant effect on the amplitude of the PSC Ca^{2+} responses from reinnervating NMJs. (b) Histograms showing the normalized PSC Ca^{2+} responses in the presence of atropine relative to control ones. Note that the mAChRs contribution (bleu) at reinnervating NMJs is significantly smaller than the ones observed at sham NMJs. *$p < .05$. NMJ, neuromuscular junction; PSC, perisynaptic Schwann cell.

± 23.98%$\Delta F/F_0$ ($N = 7$, $n = 43$), 556.60 ± 20.92%$\Delta F/F_0$ ($N = 4$, $n = 28$), and 477.70 ± 31.51%$\Delta F/F_0$ ($N = 3$, $n = 27$). This PSC muscarinic profile may reveal a glial memory of injury, at reinnervated, monoinnervated NMJs. Overall, these results argue that PSCs must properly accommodate their functional properties to ensure a reliable adaptation to changing conditions at the NMJ.
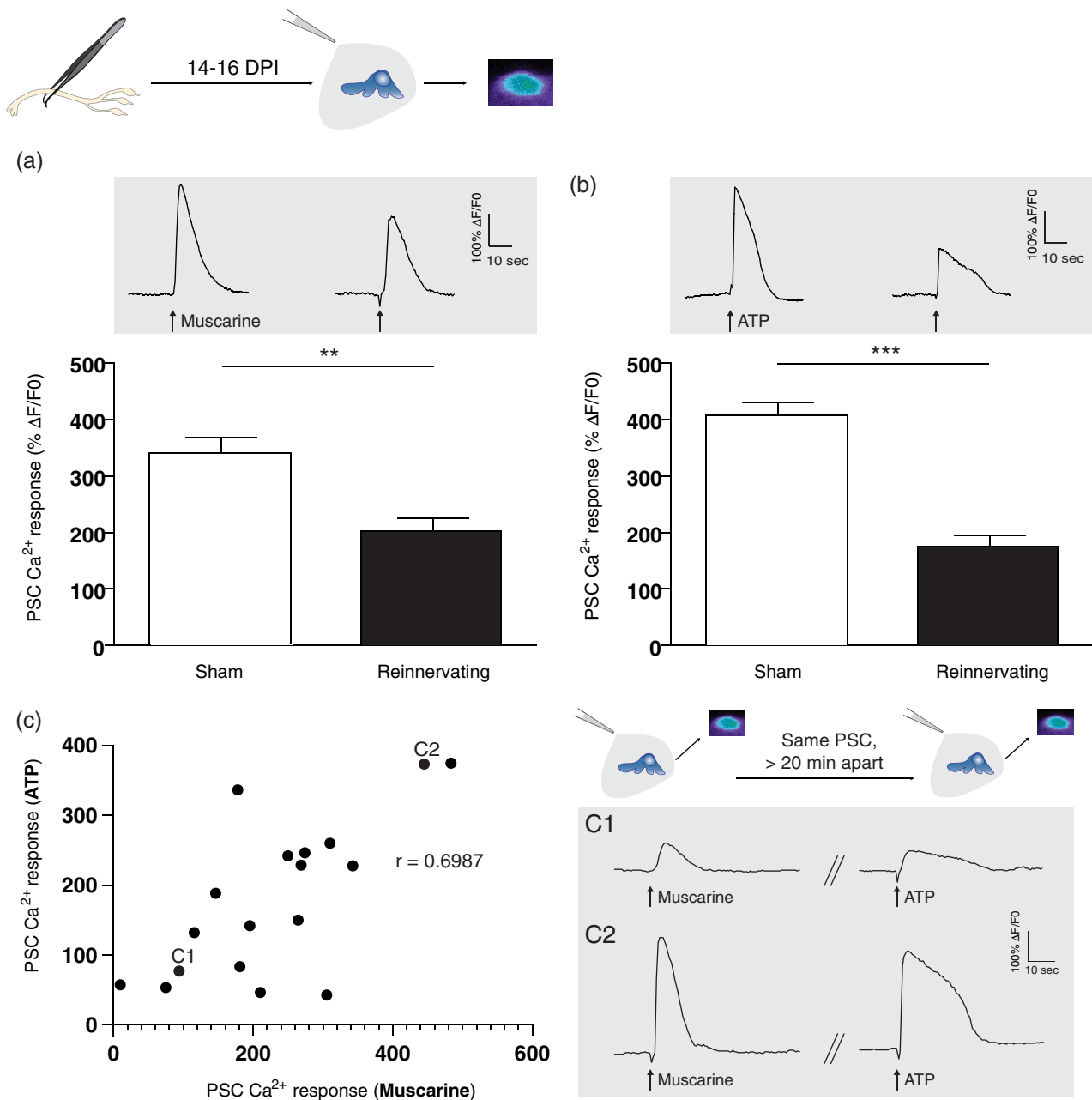
FIGURE 8 Reduced PSC mAChRs and purinergic receptors activation at reinnervating NMJs. (a) Histogram showing the mean ± SEM of PSC Ca^{2+} responses elicited by local application of muscarine (10 μm) and (b) ATP (10 μm) at sham operated (white) and reinnervating NMJs (black). Top insets (gray) illustrate representative traces elicited by respective agonists. Note that both averaged responses were significantly reduced at reinnervating NMJs compared to sham operated NMJs. (c) Graph showing the positive linear correlation of PSC Ca^{2+} responses evoked by muscarine and ATP, where each point represents a PSC. Insets (gray) illustrate representative traces elicited by both agonists, applied 20 minutes apart, in two different PSCs (c1 and c2). **$p < .01$, ***$p < .005$. NMJ, neuromuscular junction; PSC, perisynaptic Schwann cell.

4 | DISCUSSION

This study revealed that PSCs undergo functional changes in response to NMJ injury that do not reliably recapitulate the developmental NMJ maturation process. We showed that PSCs mAChRs activation was reduced during NMJ denervation and reinnervation. This reduced muscarinic signal facilitated galectin-3 expression after denervation, correlated with purinergic signal during reinnervation and was not directly associated with a number of features related to NMJ repair processes. Importantly, altered PSC properties persisted at least 60 days after injury, indicative

of a glial memory of injury. Interestingly, both PSCs muscarinic and purinergic properties were maladapted at denervated NMJs in ALS.

4.1 | Two sets of receptors, multiple functional states

PSCs must adapt to multiple synaptic contexts of the NMJ. A main constraint is to elaborate a strategy to appropriately detect the synaptic activity while maintaining or adjusting their roles at the NMJ. Our data
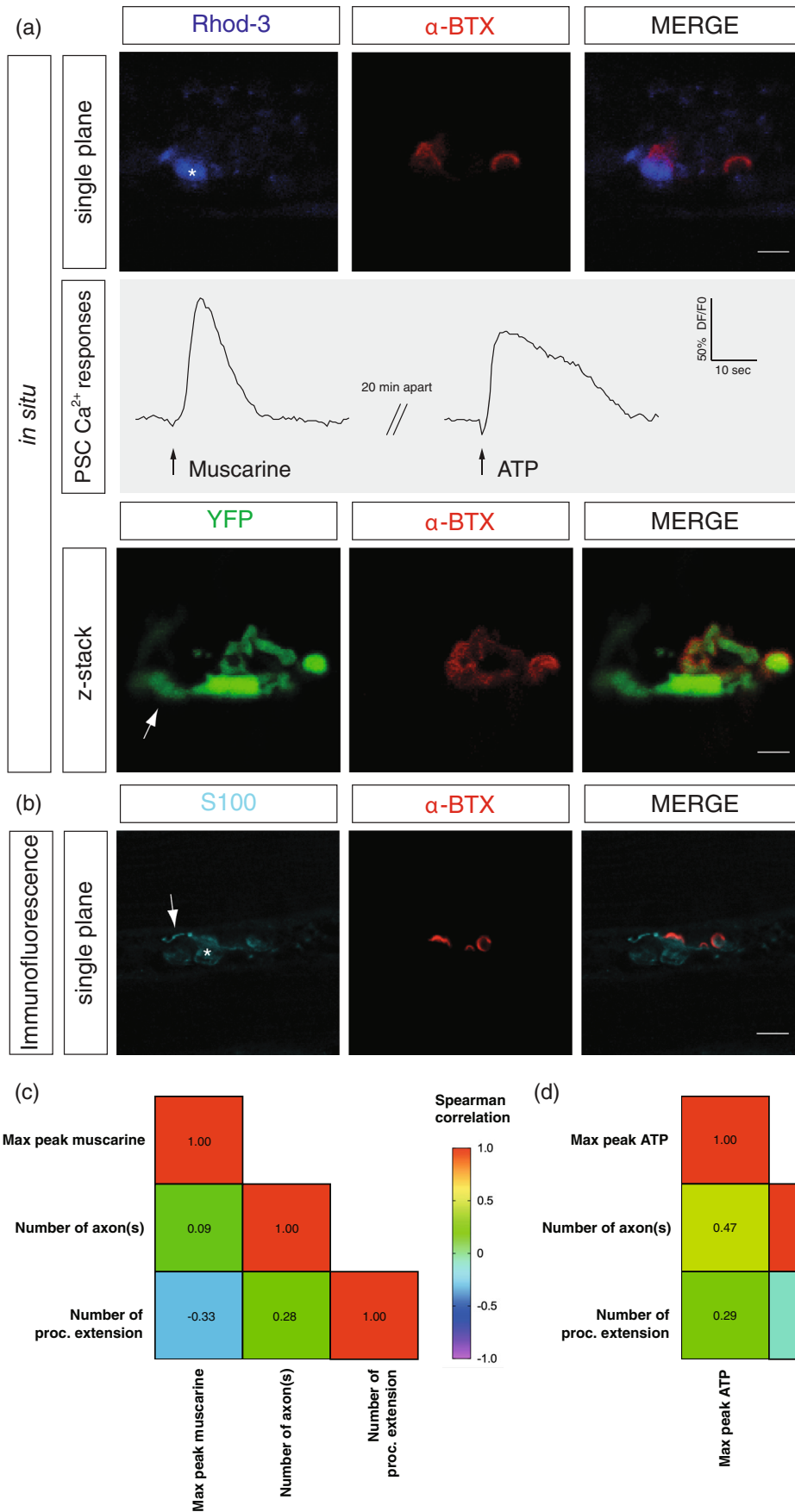
FIGURE 9 Legend on next page.

suggest that PSCs have a complex response to injury by changing the level of activation and contribution of their two main sets of receptors.

The overall muscarinic functional adaptation appears to be a key event in PSCs response to injury and the following repair. Our data are consistent with a reduced muscarinic activation when NMJ morphological/physiological plasticity is required (Ko & Robitaille, 2015), as seen at denervated, immature and reinnervating NMJs (Figures 1, 4, 7 and 8). Denervation triggered phagocytic activity revealed by galectin-3 expression in PSCs, which was reduced by muscarinic activation. The rapid removal of axonal debris is a critical step to ensure subsequent NMJ reinnervation (Kang & Lichtman, 2013). This suggests that the level of mAChR activation is a determinant for the switch of PSCs phenotype (from a maintenance to a repair mode). The remaining low muscarinic excitation in PSCs of denervated NMJs could be important for the detection of a reinnervating nerve terminal during NMJ repair. A decreased numbers of PSCs bridges following increased neuromuscular activity argue in this favor (Love et al., 2003; Tam & Gordon, 2003).

While PSCs muscarinic adaptation to injury is relatively simple (an overall reduction), our results showed that the purinergic excitability is more attuned with the synaptic context. For instance, purinergic-driven PSCs activation was reduced at reinnervating NMJs (Figure 8), but not at denervated NMJs (Figure 1), suggesting that the presence of the presynaptic element influences the purinergic adaptation. During development and reinnervation, we propose that purinergic receptors act as a gatekeeper for the synaptic regulation. At immature NMJs, PSC mAChRs and purinergic receptors normally act synergistically during synaptic communication such that mAChRs contribution is reduced when purinergic's one is enhanced (Darabid et al., 2018; Heredia et al., 2018). This would be consistent with the enhanced purinergic receptor contribution at reinnervating NMJs (Figure 4). Interestingly, the same differential synaptic plasticity at competing nerve terminals with different synaptic strength was observed after denervation (Figure 6d,f) than during postnatal development. Based on their purinergic activation, PSCs bias synaptic competition towards the stronger nerve terminal (Darabid et al., 2018). This raises the possibility that PSCs play a similar role at mature polyinnervated NMJs during reinnervation. At denervated NMJs in YFP.SOD1^{G37R} animals, the reduced purinergic activation may reflect the purinergic deregulation in ALS (Volonte et al., 2011).

4.2 | Morphological and physiological assumptions at the NMJ; caution is in order

We did not observe a simple relationship between muscarine-induced PSC Ca^{2+} responses and certain NMJ morphological features (axon and

terminal extension). This suggests that, during the reinnervation process, physiological or morphological measures alone may not be sufficient to characterize the NMJ, and one measure cannot reliably predict the other. We propose that, while the level of activation of PSC mAChRs determined the state of maintenance or repair, it may not necessarily be tributary of the presence/absence of PSC process extension or multiple axons. The observation of a persistent reduced PSC mAChRs activation at 60 DPI (Figure 10 and below), where almost all NMJs are re- and monoinnervated, is in favor of this argument. This further emphasizes the importance of caution when interpreting either the physiological or the morphological data taken individually to extrapolate to a complex situation such as reinnervation.

In addition, PSCs phenotype, including process extension, soma migration and proliferation, is likely regulated by other receptors such the neuregulin (NRG) signaling cascade (Hayworth et al., 2006). Complementary to the muscarinic and purinergic activation, PSCs response to injury and in repair could also be driven by local events such as local protein synthesis and/or neurotrophic factors. For instance, a nerve injury implies a complex regulation of lesion-associated neurotrophic factors and cytokine release (Grosheva et al., 2016) and BDNF has been implicated in the local regulation of actin at the nerve terminal (Deng et al., 2021). Interestingly, and consistent with the difference in Ca^{2+} responses generated at reinnervating and sham NMJs (Figure 7), PSCs Ca^{2+} responses evoked by endogenous release of neurotransmitters are regulated by NT-3 and BDNF (Todd et al., 2007). Whether such local regulation occurs at reinnervating NMJs will be of particular interest in future studies. Finally, the contributions of other cell types remotely associated with NMJs such as kranocytes, fibroblast-like cells caping the PSCs and positively immunostained by anti-NRG antibody, remain to be determined (Court et al., 2008).

4.3 | Time-dependent functional adaptations in response to injury; adapted PSC phenotypes for a proper NMJ and motor recovery

The timing of events after a nerve injury may influence the success of reinnervation and recovery of the motor function. For instance, the degree of recovery is inversely correlated with the duration of denervation (Kang et al., 2014; Stefancic et al., 2016) while reinnervation must occur within a critical time window for a successful motor recovery (Ma et al., 2011). Hence, understanding PSCs functional adaptation in a time-dependent manner during the denervation/reinnervation process should help understand and favor NMJ repair and motor recovery.

FIGURE 9 No correlation between PSC Ca^{2+} responses and the number of axon(s) or process(es) extension at reinnervating NMJs. (a) Upper panel: False color confocal images of a single plane focusing on one NMJ with one PSC loaded with the Rhod-3 Ca^{2+} indicator (blue) caping the nAChRs (α-BTX, red). Middle panel (gray): PSC Ca^{2+} responses elicited by muscarine (10 μm) or ATP (10 μm). Lower panel: During the same in situ experiment, the number of axon(s) was evaluated with the false color confocal image of z-stack focusing on the same NMJ with the YFP signal (green) and the α-BTX (red) staining. Note the presence of a single axon at this NMJ. (b) False color confocal image of a single plane focusing on the same PSC (S100, cyan, asterisk) illustrated in (a) caping the same nAChRs (α-BTX, red). Note the presence of a process extension (arrow). (c) Correlation matrix depicting the lack of relation between PSC Ca^{2+} responses evoked by muscarine (10 μm) or (d) ATP (10 μm) and the number of axon(s) and process(es) extension. Scale bars: 10 μm. NMJ, neuromuscular junction; PSC, perisynaptic Schwann cell.
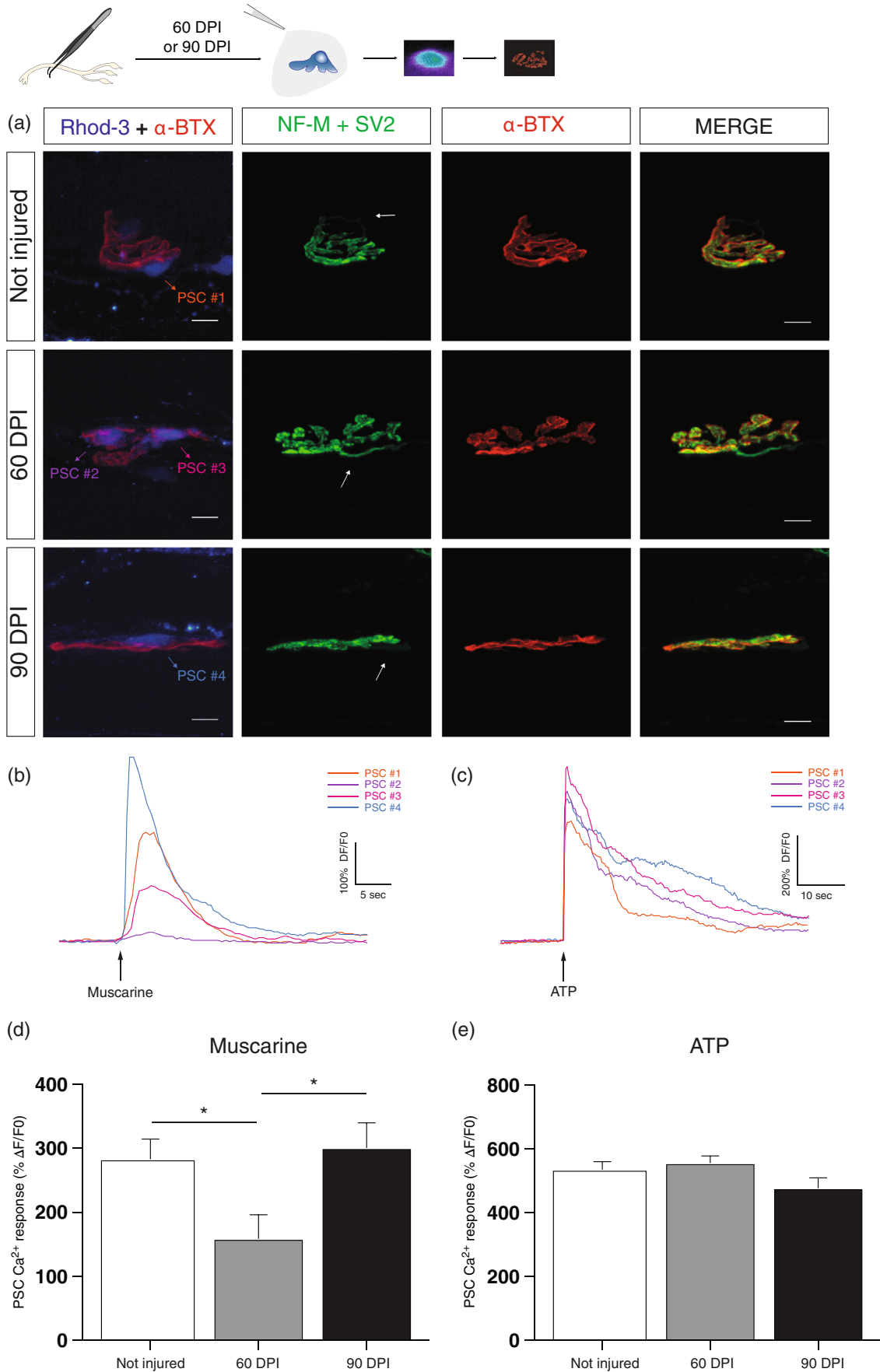
FIGURE 10 Legend on next page.

The involvement of PSCs in several steps during the denervation/reinnervation processes implies a rapid adaptation, in phase with their associated NMJ to promote and facilitate the reinnervation and motor recovery. First, PSCs must detect the injury, which directly depends on their capacity to detect synaptic activity, particularly through mAChRs (Georgiou et al., 1999). Second, they must adapt their functional properties to allow their phenotype to switch from a maintenance to a repair mode (Ko & Robitaille, 2015). This repair phenotype appears required for debris clearance (galectin-3 expression), a necessary step to allow the regrowing axon to invade the endplate (Kang & Lichtman, 2013). Third, PSCs undergo morphological changes that facilitate NMJ repair and its functional support (e.g., PSCs processes that guide sprouts of nerve terminal at innervated NMJs towards denervated ones) (Magill et al., 2007; O'Malley et al., 1999; Reynolds & Woolf, 1992; Son & Thompson, 1995a, 1995b). Fourth, PSCs release factors that facilitate NMJ recovery. For instance, until the axons recontact the NMJ, PSCs can help to maintain endplate organization in place by releasing ACh (Dennis & Miledi, 1974), consistent with the importance to maintain nAChRs clusters for functional recovery (Li et al., 2020). This is also consistent with PSCs release of matrix metalloproteinase 3 (MMP-3), the major enzyme responsible for the degradation of agrin, an important factor for the preservation of the integrity of postsynaptic endplates (Chao et al., 2013). PSCs can also promote motor nerve terminal growth via the release of CXCL12α (Negro et al., 2017). Fifth, during synaptic competition at reinnervating NMJs, PSCs detect synaptic activity of polyinnervated synaptic inputs, and could bias the modulation towards the strongest nerve terminal input (Darabid et al., 2018). Sixth, PSCs can influence the pattern of muscle reinnervation (Kang et al., 2019) and the remodeling of the reinnervating NMJs by either the removal or addition of postsynaptic receptor sites (Kang et al., 2014). Finally, PSCs must promote the stabilization, maintenance and regulation of the synaptic activity of the newly re-formed NMJ (Reddy et al., 2003). Importantly, the presence of PSCs is essential for NMJ maintenance and function since a decline in the number of Schwann cells results in a decline in NMJ numbers and coincides with irreversible changes of motor function after a nerve injury (Li et al., 2020). Hence, altering PSCs functional properties in a time-specific matter during reinnervation processes would help establish their respectives roles and establish the importance of any of these steps discussed above. The recent publications of a specific tool to specifically target PSCs could prove valuable in that matter (Castro et al., 2020).

4.4 | Glial memory of injury at the NMJ

We observed a long-lasting reduced muscarinic signaling following injury (Figure 10). We propose that this represents a glial memory of injury, keeping the PSCs in an alarm/awareness state. This not only challenges the assumption that PSC properties are restored rapidly after NMJ reinnervation, but also, gives new perspectives on PSCs implications for a complete recovery. This may favor PSCs to stay in a repair mode by either releasing neurotrophic factors to stabilize the reinnervated NMJ. This may also allow them to be more sensitive or more rapidly adaptive to subsequent injury and amenable to adjustments to the general motor recovery. For instance, it was reported that SOL isometric twitch tension of young animals with L5 root section had returned to control values after 60 days (Jacob & Robbins, 1990). This PSC memory of injury might be comparable to microglia in the CNS whereby proliferation and migration return to baseline approximately 2 months after injury (Polgar et al., 2005; Tay et al., 2017). In a disease like ALS, where there are multiple cycles of denervation and reinnervation (Martineau et al., 2018), we argue that the lack of muscarinic adaptation observed at denervated NMJs (Figure 3) will prevent PSCs from adopting the proper phenotype to deal with such dynamic NMJ plasticity. A proper evaluation of the involvement of the PSC mAChRs in NMJ reinnervation still awaits further clarification. It will be also of interest to evaluate if other regulating mechanisms are also under the control of such long-term modulation.

4.5 | Altered PSC properties in ALS

Many PSCs abnormalities have been reported in ALS that could impinge on their response to injury. For instance, PSCs have an increased mAChR-dependent activity (transiently in a fast twitch muscle; Arbour et al., 2015; Martineau et al., 2020), release a chemorepellent substance for axon at vulnerable NMJs (De Winter et al., 2006) and show a maladapted galectin-3 expression on denervated NMJs (Martineau et al., 2020). They also form muddled, untargeted processes that fail to guide nerve terminal sprouting appropriately (Martineau et al., 2020). Finally, fewer PSCs per NMJ have been reported and an altered phenotype before and after NMJ denervation (Carrasco, Bahr, et al., 2016; Carrasco, Seburn, & Pinter, 2016; Harrison & Rafuse, 2020). All together, these data converge towards the same end result that PSCs' phenotype is incompatible with NMJ repair and may directly impact NMJ viability during the progression of ALS.

Whether the delay in NMJ reinnervation following axonal injury in ALS or the very susceptibility to NMJ loss in ALS are directly related to PSCs or are related to intrinsic neuronal/axonal defects remains an open question. Evidence points towards the fact that

FIGURE 10 Reduced PSCs mAChRs activation persists after reinnervation. (a) False color confocal images of NMJs from Not injured, 60 and 90 DPI animals. During the Ca^{2+} imaging experiment, PSCs were loaded with the Rhod-3 Ca^{2+} indicator (blue) and postsynaptic nAChRs with α-BTX (red). Subsequently, SOL NMJs were immunolabeled for the nerve terminals (NF-M + SV2, green) and postsynaptic nAChRs (α-BTX, red). Note that all reinnervated NMJs were monoinnervated (arrows). (b) Representative Ca^{2+} traces elicited by muscarine (10 μm) and (c) ATP (10 μm) by each PSC illustrated in (a). (d) Histogram showing the mean ± SEM of PSC Ca^{2+} responses elicited by local application of muscarine (10 μm) and (e) ATP (10 μm) at control (white), 60 DPI (gray) and 90 DPI (black) animals. Scale bars: 10 μm. *$p < .05$. NMJ, neuromuscular junction; PSC, perisynaptic Schwann cell.

several core NMJ mechanisms are altered and reflect NMJ susceptibility in ALS, affecting all three synaptic elements (Arbour et al., 2015; Cantor et al., 2018; Martineau et al., 2020; Tremblay et al., 2017). Hence, a more integrated vision of this synapse is needed for a better understanding of the disease and the development of combined therapeutic approaches.

In conclusion, we observed specific PSC mAChRs and purinergic receptors adaptations in response to NMJ maturation, denervation/reinnervation and in disease. These adaptations appear to be fundamental and distinct properties of PSCs that allow them to perform their dynamic and multifaceted roles at the NMJ. Our results further suggest that PSC mAChRs downregulation may be a general approach to facilitate NMJ repair in adulthood. Results from this study are important not only for understanding denervation and reinnervation mechanisms following NMJ injury but also similar events that occur in normal aging or neurodegenerative diseases such as ALS.

CONFLICT OF INTEREST

The authors declare no conflict of interest.

AUTHOR CONTRIBUTORS

Anna P. Perez-Gonzalez, Isabelle Rousse, Danielle Arbour and Richard Robitaille conceived and designed the project. **Anna P. Perez-Gonzalez, Frédéric Provost, Isabelle Rousse, Roberta Piovesana, Ouafa Benzina, Houssam Darabid, Benoit Lamoureux and Danielle Arbour** acquired the data. **Anna P. Perez-Gonzalez, Frédéric Provost, Isabelle Rousse, Roberta Piovesana, Ouafa Benzina, Houssam Darabid, Benoit Lamoureux, Yu Shi Wang, Danielle Arbour and Richard Robitaille** analyzed and interpreted the data. **Anna P. Perez-Gonzalez, Isabelle Rousse, Danielle Arbour and Richard Robitaille** wrote the paper.

DATA AVAILABILITY STATEMENT

The data that support the findings of this study are available from the corresponding author upon reasonable request.

ORCID

Anna P. Perez-Gonzalez 🔸 https://orcid.org/0000-0002-5588-8233
Frédéric Provost 🔸 https://orcid.org/0000-0002-2432-7580
Danielle Arbour 🔸 https://orcid.org/0000-0002-7268-1488
Richard Robitaille 🔸 https://orcid.org/0000-0001-6628-0146

REFERENCES

Arbour, D., Tremblay, E., Martineau, E., Julien, J. P., & Robitaille, R. (2015). Early and persistent abnormal decoding by glial cells at the neuromuscular junction in an ALS model. *The Journal of Neuroscience*, 35(2), 688–706. https://doi.org/10.1523/JNEUROSCI.1379-14.2015

Balice-Gordon, R. J., & Lichtman, J. W. (1993). In vivo observations of pre- and postsynaptic changes during the transition from multiple to single innervation at developing neuromuscular junctions. *The Journal of Neuroscience*, 13(2), 834–855.

Belair, E. L., Vallee, J., & Robitaille, R. (2010). In vivo long-term synaptic plasticity of glial cells. *The Journal of Physiology*, 588(Pt 7), 1039–1056. https://doi.org/10.1113/jphysiol.2009.178988

Cantor, S., Zhang, W., Delestree, N., Remedio, L., Mentis, G. Z., & Burden, S. J. (2018). Preserving neuromuscular synapses in ALS by stimulating MuSK with a therapeutic agonist antibody. *eLife*, 7, e34375. https://doi.org/10.7554/eLife.34375

Carrasco, D. I., Bahr, B. A., Seburn, K. L., & Pinter, M. J. (2016). Abnormal response of distal Schwann cells to denervation in a mouse model of motor neuron disease. *Experimental Neurology*, 278, 116–126. https://doi.org/10.1016/j.expneurol.2016.02.002

Carrasco, D. I., Seburn, K. L., & Pinter, M. J. (2016). Altered terminal Schwann cell morphology precedes denervation in SOD1 mice. *Experimental Neurology*, 275(Pt 1), 172–181. https://doi.org/10.1016/j.expneurol.2015.09.014

Castonguay, A., & Robitaille, R. (2001). Differential regulation of transmitter release by presynaptic and glial Ca2+ internal stores at the neuromuscular synapse. *The Journal of Neuroscience*, 21(6), 1911–1922.

Castro, R., Taetzsch, T., Vaughan, S. K., Godbe, K., Chappell, J., Settlage, R. E., & Valdez, G. (2020). Specific labeling of synaptic schwann cells reveals unique cellular and molecular features. *eLife*, 9, 1–19. https://doi.org/10.7554/eLife.56935

Chao, T., Frump, D., Lin, M., Caiozzo, V. J., Mozaffar, T., Steward, O., & Gupta, R. (2013). Matrix metalloproteinase 3 deletion preserves denervated motor endplates after traumatic nerve injury. *Annals of Neurology*, 73(2), 210–223. https://doi.org/10.1002/ana.23781

Court, F. A., Gillingwater, T. H., Melrose, S., Sherman, D. L., Greenshields, K. N., Morton, A. J., Harris, J. B., Willison, H. J., & Ribchester, R. R. (2008). Identity, developmental restriction and reactivity of extralaminar cells capping mammalian neuromuscular junctions. *Journal of Cell Science*, 121(Pt 23), 3901–3911. https://doi.org/10.1242/jcs.031047

Darabid, H., Arbour, D., & Robitaille, R. (2013). Glial cells decipher synaptic competition at the mammalian neuromuscular junction. *The Journal of Neuroscience*, 33(4), 1297–1313. https://doi.org/10.1523/JNEUROSCI.2935-12.2013

Darabid, H., Perez-Gonzalez, A. P., & Robitaille, R. (2014). Neuromuscular synaptogenesis: Coordinating partners with multiple functions. *Nature Reviews. Neuroscience*, 15(11), 703–718.

Darabid, H., St-Pierre-See, A., & Robitaille, R. (2018). Purinergic-dependent glial regulation of synaptic plasticity of competing terminals and synapse elimination at the neuromuscular junction. *Cell Reports*, 25(8), 2070–2082 e2076. https://doi.org/10.1016/j.celrep.2018.10.075

de Winter, F., Vo, T., Stam, F. J., Wisman, L. A., Bär, P. R., Niclou, S. P., van Muiswinkel, F., & Verhaagen, J. (2006). The expression of the chemorepellent Semaphorin 3A is selectively induced in terminal Schwann cells of a subset of neuromuscular synapses that display limited anatomical plasticity and enhanced vulnerability in motor neuron disease. *Molecular and Cellular Neurosciences*, 32(1–2), 102–117. https://doi.org/10.1016/j.mcn.2006.03.002

Del Castillo, J., & Katz, B. (1954). Quantal components of the end-plate potential. *The Journal of Physiology*, 124(3), 560–573. https://doi.org/10.1113/jphysiol.1954.sp005129

Deng, C., Moradi, M., Reinhard, S., Ji, C., Jablonka, S., Hennlein, L., Lüningschrör, P., Doose, S., Sauer, M., & Sendtner, M. (2021). Dynamic remodeling of ribosomes and endoplasmic reticulum in axon terminals of motoneurons. *Journal of Cell Science*, 134(22), 1–16. https://doi.org/10.1242/jcs.258785

Dennis, M. J., & Miledi, R. (1974). Electrically induced release of acetylcholine from denervated Schwann cells. *The Journal of Physiology*, 237(2), 431–452. https://doi.org/10.1113/jphysiol.1974.sp010490

Duregotti, E., Negro, S., Scorzeto, M., Zornetta, I., Dickinson, B. C., Chang, C. J., Montecucco, C., & Rigoni, M. (2015). Mitochondrial alarmins released by degenerating motor axon terminals activate perisynaptic Schwann cells. *Proceedings of the National Academy of Sciences of the United States of America*, 112(5), E497–E505. https://doi.org/10.1073/pnas.1417108112

Feng, G., Mellor, R. H., Bernstein, M., Keller-Peck, C., Nguyen, Q. T., Wallace, M., Nerbonne, J. M., Lichtman, J. W., & Sanes, J. R. (2000). Imaging neuronal subsets in transgenic mice expressing multiple spectral variants of GFP. *Neuron*, 28(1), 41–51. https://doi.org/10.1016/s0896-6273(00)00084-2

Georgiou, J., Robitaille, R., & Charlton, M. P. (1999). Muscarinic control of cytoskeleton in perisynaptic glia. *The Journal of Neuroscience*, 19(10), 3836–3846.

Georgiou, J., Robitaille, R., Trimble, W. S., & Charlton, M. P. (1994). Synaptic regulation of glial protein expression in vivo. *Neuron*, 12(2), 443–455. https://doi.org/10.1016/0896-6273(94)90284-4

Grosheva, M., Nohroudi, K., Schwarz, A., Rink, S., Bendella, H., Sarikcioglu, L., Klimaschewski, L., Gordon, T., & Angelov, D. N. (2016). Comparison of trophic factors' expression between paralyzed and recovering muscles after facial nerve injury. A quantitative analysis in time course. *Experimental Neurology*, 279, 137–148. https://doi.org/10.1016/j.expneurol.2016.02.020

Harrison, J. M., & Rafuse, V. F. (2020). Muscle fiber-type specific terminal Schwann cell pathology leads to sprouting deficits following partial denervation in SOD1(G93A) mice. *Neurobiology of Disease*, 145, 1–15. https://doi.org/10.1016/j.nbd.2020.105052

Hayworth, C. R., Moody, S. E., Chodosh, L. A., Krieg, P., Rimer, M., & Thompson, W. J. (2006). Induction of neuregulin signaling in mouse schwann cells in vivo mimics responses to denervation. *The Journal of Neuroscience*, 26(25), 6873–6884. https://doi.org/10.1523/JNEUROSCI.1086-06.2006

Heredia, D. J., Feng, C. Y., Hennig, G. W., Renden, R. B., & Gould, T. W. (2018). Activity-induced ca(2+) signaling in perisynaptic Schwann cells of the early postnatal mouse is mediated by P2Y1 receptors and regulates muscle fatigue. *eLife*, 7, 1–27. https://doi.org/10.7554/eLife.30839

Hirata, K., Zhou, C., Nakamura, K., & Kawabuchi, M. (1997). Postnatal development of Schwann cells at neuromuscular junctions, with special reference to synapse elimination. *Journal of Neurocytology*, 26(12), 799–809. https://doi.org/10.1023/a:1018570500052

Jacob, J. M., & Robbins, N. (1990). Differential effects of age on neuromuscular transmission in partially denervated mouse muscle. *The Journal of Neuroscience*, 10(5), 1522–1529.

Jahromi, B. S., Robitaille, R., & Charlton, M. P. (1992). Transmitter release increases intracellular calcium in perisynaptic Schwann cells in situ. *Neuron*, 8(6), 1069–1077. https://doi.org/10.1016/0896-6273(92)90128-z

Kang, H., & Lichtman, J. W. (2013). Motor axon regeneration and muscle reinnervation in young adult and aged animals. *The Journal of Neuroscience*, 33(50), 19480–19491. https://doi.org/10.1523/JNEUROSCI.4067-13.2013

Kang, H., Tian, L., Mikesh, M., Lichtman, J. W., & Thompson, W. J. (2014). Terminal Schwann cells participate in neuromuscular synapse remodeling during reinnervation following nerve injury. *The Journal of Neuroscience*, 34(18), 6323–6333. https://doi.org/10.1523/JNEUROSCI.4673-13.2014

Kang, H., Tian, L., & Thompson, W. J. (2019). Schwann cell guidance of nerve growth between synaptic sites explains changes in the pattern of muscle innervation and remodeling of synaptic sites following peripheral nerve injuries. *The Journal of Comparative Neurology*, 527(8), 1388–1400. https://doi.org/10.1002/cne.24625

Ko, C. P., & Robitaille, R. (2015). Perisynaptic Schwann cells at the neuromuscular synapse: Adaptable, multitasking glial cells. *Cold Spring Harbor Perspectives in Biology*, 7(10), a020503. https://doi.org/10.1101/cshperspect.a020503

Li, L., Yokoyama, H., Kaburagi, H., Hirai, T., Tsuji, K., Enomoto, M., Wakabayashi, Y., & Okawa, A. (2020). Remnant neuromuscular junctions in denervated muscles contribute to functional recovery in delayed peripheral nerve repair. *Neural Regeneration Research*, 15(4), 731–738. https://doi.org/10.4103/1673-5374.266925

Love, F. M., Son, Y. J., & Thompson, W. J. (2003). Activity alters muscle reinnervation and terminal sprouting by reducing the number of Schwann cell pathways that grow to link synaptic sites. *Journal of Neurobiology*, 54(4), 566–576. https://doi.org/10.1002/neu.10191

Ma, C. H., Omura, T., Cobos, E. J., Latrémolière, A., Ghasemlou, N., Brenner, G. J., van Veen, E., Barrett, L., Sawada, T., Gao, F., Coppola, G., Gertler, F., Costigan, M., Geschwind, D., & Woolf, C. J. (2011). Accelerating axonal growth promotes motor recovery after peripheral nerve injury in mice. *The Journal of Clinical Investigation*, 121(11), 4332–4347. https://doi.org/10.1172/JCI58675

Magill, C. K., Tong, A., Kawamura, D., Hayashi, A., Hunter, D. A., Parsadanian, A., Mackinnon, S. E., & Myckatyn, T. M. (2007). Reinnervation of the tibialis anterior following sciatic nerve crush injury: A confocal microscopic study in transgenic mice. *Experimental Neurology*, 207(1), 64–74. https://doi.org/10.1016/j.expneurol.2007.05.028

Martineau, E., Arbour, D., Vallee, J., & Robitaille, R. (2020). Properties of glial cell at the neuromuscular junction are incompatible with synaptic repair in the SOD1(G37R) ALS mouse model. *The Journal of Neuroscience*, 40(40), 7759–7777. https://doi.org/10.1523/JNEUROSCI.1748-18.2020

Martineau, E., Di Polo, A., Vande Velde, C., & Robitaille, R. (2018). Dynamic neuromuscular remodeling precedes motor-unit loss in a mouse model of ALS. *eLife*, 7, 1–19. https://doi.org/10.7554/eLife.41973

Negro, S., Lessi, F., Duregotti, E., Aretini, P., la Ferla, M., Franceschi, S., Menicagli, M., Bergamin, E., Radice, E., Thelen, M., Megighian, A., Pirazzini, M., Mazzanti, C. M., Rigoni, M., & Montecucco, C. (2017). CXCL12alpha/SDF-1 from perisynaptic Schwann cells promotes regeneration of injured motor axon terminals. *EMBO Molecular Medicine*, 9(8), 1000–1010. https://doi.org/10.15252/emmm.201607257

O'Malley, J. P., Waran, M. T., & Balice-Gordon, R. J. (1999). In vivo observations of terminal Schwann cells at normal, denervated, and reinnervated mouse neuromuscular junctions. *Journal of Neurobiology*, 38(2), 270–286.

Polgar, E., Hughes, D. I., Arham, A. Z., & Todd, A. J. (2005). Loss of neurons from laminas I-III of the spinal dorsal horn is not required for development of tactile allodynia in the spared nerve injury model of neuropathic pain. *The Journal of Neuroscience*, 25(28), 6658–6666. https://doi.org/10.1523/JNEUROSCI.1490-05.2005

Reddy, L. V., Koirala, S., Sugiura, Y., Herrera, A. A., & Ko, C. P. (2003). Glial cells maintain synaptic structure and function and promote development of the neuromuscular junction in vivo. *Neuron*, 40(3), 563–580. https://doi.org/10.1016/s0896-6273(03)00682-2

Reichert, F., Saada, A., & Rotshenker, S. (1994). Peripheral nerve injury induces Schwann cells to express two macrophage phenotypes: Phagocytosis and the galactose-specific lectin MAC-2. *The Journal of Neuroscience*, 14(5 Pt 2), 3231–3245.

Reynolds, M. L., & Woolf, C. J. (1992). Terminal Schwann cells elaborate extensive processes following denervation of the motor endplate. *Journal of Neurocytology*, 21(1), 50–66. https://doi.org/10.1007/bf01206897

Rich, M. M., & Lichtman, J. W. (1989). In vivo visualization of pre- and postsynaptic changes during synapse elimination in reinnervated mouse muscle. *The Journal of Neuroscience*, 9(5), 1781–1805.

Robitaille, R. (1998). Modulation of synaptic efficacy and synaptic depression by glial cells at the frog neuromuscular junction. *Neuron*, 21(4), 847–855. https://doi.org/10.1016/s0896-6273(00)80600-5

Rochon, D., Rousse, I., & Robitaille, R. (2001). Synapse-glia interactions at the mammalian neuromuscular junction. *The Journal of Neuroscience*, *21*(11), 3819–3829.

Rousse, I., St-Amour, A., Darabid, H., & Robitaille, R. (2010). Synapse-glia interactions are governed by synaptic and intrinsic glial properties. *Neuroscience*, *167*(3), 621–632. https://doi.org/10.1016/j.neuroscience.2010.02.036

Son, Y. J., & Thompson, W. J. (1995a). Nerve sprouting in muscle is induced and guided by processes extended by Schwann cells. *Neuron*, *14*(1), 133–141. https://doi.org/10.1016/0896-6273(95)90247-3

Son, Y. J., & Thompson, W. J. (1995b). Schwann cell processes guide regeneration of peripheral axons. *Neuron*, *14*(1), 125–132. https://doi.org/10.1016/0896-6273(95)90246-5

Stefancic, M., Vidmar, G., & Blagus, R. (2016). Long-term recovery of muscle strength after denervation in the fibular division of the sciatic nerve. *Muscle & Nerve*, *54*(4), 702–708. https://doi.org/10.1002/mus.25103

Tam, S. L., & Gordon, T. (2003). Neuromuscular activity impairs axonal sprouting in partially denervated muscles by inhibiting bridge formation of perisynaptic Schwann cells. *Journal of Neurobiology*, *57*(2), 221–234. https://doi.org/10.1002/neu.10276

Tay, T. L., Mai, D., Dautzenberg, J., Fernández-Klett, F., Lin, G., Sagar, Datta, M., Drougard, A., Stempfl, T., Ardura-Fabregat, A., Staszewski, O., Margineanu, A., Sporbert, A., Steinmetz, L. M., Pospisilik, J. A., Jung, S., Priller, J., Grün, D., Ronneberger, O., & Prinz, M. (2017). A new fate mapping system reveals context-dependent random or clonal expansion of microglia. *Nature Neuroscience*, *20*(6), 793–803. https://doi.org/10.1038/nn.4547

Todd, K. J., Auld, D. S., & Robitaille, R. (2007). Neurotrophins modulate neuron-glia interactions at a vertebrate synapse. *The European Journal of Neuroscience*, *25*(5), 1287–1296. https://doi.org/10.1111/j.1460-9568.2007.05385.x

Todd, K. J., Darabid, H., & Robitaille, R. (2010). Perisynaptic glia discriminate patterns of motor nerve activity and influence plasticity at the neuromuscular junction. *The Journal of Neuroscience*, *30*(35), 11870–11882. https://doi.org/10.1523/JNEUROSCI.3165-10.2010

Tremblay, E., Martineau, E., & Robitaille, R. (2017). Opposite synaptic alterations at the neuromuscular junction in an ALS mouse model: When motor units matter. *The Journal of Neuroscience*, *37*(37), 8901–8918. https://doi.org/10.1523/JNEUROSCI.3090-16.2017

Volonte, C., Apolloni, S., Carri, M. T., & D'Ambrosi, N. (2011). ALS: Focus on purinergic signalling. *Pharmacology & Therapeutics*, *132*(1), 111–122. https://doi.org/10.1016/j.pharmthera.2011.06.002

Wong, P. C., Pardo, C. A., Borchelt, D. R., Lee, M. K., Copeland, N. G., Jenkins, N. A., Sisodia, S. S., Cleveland, D. W., & Price, D. L. (1995). An adverse property of a familial ALS-linked SOD1 mutation causes motor neuron disease characterized by vacuolar degeneration of mitochondria. *Neuron*, *14*(6), 1105–1116. https://doi.org/10.1016/0896-6273(95)90259-7

Wright, M. C., Potluri, S., Wang, X., Dentcheva, E., Gautam, D., Tessler, A., Wess, J., Rich, M. M., & Son, Y. J. (2009). Distinct muscarinic acetylcholine receptor subtypes contribute to stability and growth, but not compensatory plasticity, of neuromuscular synapses. *The Journal of Neuroscience*, *29*(47), 14942–14955. https://doi.org/10.1523/JNEUROSCI.2276-09.2009